Influences of downward transport and photochemistry on surface ozone over East Antarctica during austral summer: in situ observations and model simulations

Imran A. Girach[1,2*], Narendra Ojha[3], Prabha R. Nair[4,2], Kandula V. Subrahmanyam[5,2], Neelakantan Koushik[6], Mohammed M. Nazeer[6], Nadimpally Kiran Kumar[6], Surendran Nair Suresh Babu[6], Jos Lelieveld[7], and Andrea Pozzer[7,8*]

[1]Space Applications Centre, Indian Space Research Organisation, Ahmedabad 380015, India
[2]*Formerly at* Space Physics Laboratory, Vikram Sarabhai Space Centre, Thiruvananthapuram 695022, India
[3]Space and Atmospheric Sciences Division, Physical Research Laboratory, Ahmedabad 380009, India
[4]TC 95/1185, Aiswarya Gardens, Kumarapuram, Thiruvananthapuram - 695011, India
[5]National Remote Sensing Centre, Indian Space Research Organisation, Hyderabad 500015, India
[6]Space Physics Laboratory, Vikram Sarabhai Space Centre, Thiruvananthapuram 695022, India
[7]Department of Atmospheric Chemistry, Max Planck Institute for Chemistry, Mainz 55128, Germany
[8]Climate and Atmosphere Research Center, The Cyprus Institute, Nicosia, Cyprus

Correspondence to: Imran A. Girach (imran.girach@gmail.com) and Andrea Pozzer (andrea.pozzer@mpic.de)

Abstract. Studies of atmospheric trace gases in remote, pristine environments are critical for assessing the accuracy of climate models and advancing our understanding of natural processes and global changes. We investigated the surface ozone (O_3) variability over East Antarctica during the austral summer of 2015–2017 by combining surface and balloon-borne measurements at the Indian station Bharati (69.4° S, 76.2° E, ~35 m above mean sea level) with EMAC atmospheric chemistry-climate model simulations. The model reproduced the observed surface O_3 level (18.8 ± 2.3 nmol mol^{-1}) with negligible bias and captured much of the variability (R=0.5). Model simulated tropospheric O_3 profiles were in reasonable agreement with balloon-borne measurements (mean bias: 2~~3~~–1~~1~~2 nmol mol^{-1}). Our analysis of a stratospheric tracer in the model showed that about 4~~10~~–5~~0~~1% of surface O_3 over the entire Antarctic region was of stratospheric origin. Events of enhanced O_3 (~4–10 nmol mol^{-1}) were investigated by combining O_3 vertical profiles and air mass back trajectories, which revealed the rapid descent of O_3-rich air towards the surface. The photochemical loss of O_3 through its photolysis (followed by $H_2O+O(^1D)$) and reaction with hydroperoxyl radicals (O_3+HO_2) dominated over production from precursor gases ($NO+HO_2$ and $NO+CH_3O_2$) resulting in overall net O_3 loss during the austral summer. Interestingly, the east coastal region, including the Bharati station, tends to act as a stronger chemical sink of O_3 (~190 pmol mol^{-1} d^{-1}) than adjacent land and ocean regions (by ~100 pmol

mol^{-1} d^{-1}). This is attributed to reverse latitudinal gradients between H_2O and $O(^1D)$, whereby O_3 loss through photolysis ($H_2O+O(^1D)$) reaches a maximum over the east coast. Further, the net photochemical loss at the surface is counterbalanced by downward O_3 fluxes, maintaining the observed O_3 levels. The O_3 diurnal variability of ~1.5 nmol mol^{-1} was a manifestation of combined effects of mesoscale wind changes and up- and downdrafts, in addition to the net photochemical loss. The study provides valuable insights into the intertwined dynamical and chemical processes governing the O_3 levels and variability over East Antarctica.

1   Introduction

Tropospheric ozone (O_3) plays a pivotal role in governing the atmospheric oxidation capacity, and influences air quality and climate warming (Seinfeld and Pandis, 1998). The major source of O_3 in the troposphere is its photochemical formation involving precursors such as nitrogen oxides (NO_x), carbon monoxide (CO) and non-methane hydrocarbons (NMHCs; Lelieveld and Dentener, 2000). The contribution of downward transport from the stratosphere is generally minor near the surface, although it can be significant at middle to high latitudes (Stohl et al., 2003). Numerous studies have investigated the chemistry and dynamics of tropospheric O_3 and the roles of local to synoptic-scale processes (e.g., boundary layer height variation, horizontal and vertical transport, etc.; Nguyen et al., 2022; Young et al., 2018). Investigations of O_3 variations in remote pristine environments, isolated from major anthropogenic influences, are essential to understand the global changes in atmospheric composition, the role of natural processes including downward transport from the stratosphere, and photo-denitrification of the snowpack (Jones et al., 2001). In this regard, the observations over environments such as Antarctica are extremely valuable and can provide insights into the global background atmosphere, besides providing data to test the results of chemistry-climate models. The mean surface O_3 over the Antarctic region was observed to be lower by nearly 5 nmol mol^{-1} than that over the Arctic polar region (Helmig et al., 2007). Surface O_3 shows a pronounced seasonality (~15–20 nmol mol^{-1} amplitude) with a summer minimum and a winter maximum over Antarctica, accompanied by periodic fluctuations associated with long-range transport (Kumar et al., 2021; Legrand et al., 2016; Oltmans and Komhyr, 1976; Winkler et al., 1992). In line with global increases in tropospheric O_3 due to the enhanced anthropogenic emissions since the pre-industrial era and impacts of climate warming (Wang et al., 2022; Murazaki and Hess, 2006; Lelieveld et al., 2004), an increasing positive trend

(0.08–0.13<0.2 nmol mol^{-1} y^{-1} over Syowa, Arrival Heights, Neumayer, and South Pole) in surface O$_3$ has also been reported from Antarctica (Kumar et al., 2021).

Previous studies have investigated the long-term, inter-annual, seasonal and diurnal variations in surface O$_3$ over Antarctica (Legrand et al., 2009, 2016), as well as the role of horizontal transport (Tian et al., 2022) and chemistry including that of radicals (Preunkert et al., 2012), halogen driven O$_3$ depletion (Tarasick and Bottenheim, 2002; Jones et al., 2013), and stratospheric intrusions (Das et al., 2020). Antarctic observations have provided evidence of widespread O$_3$ production during austral spring and summertime, affecting all stations through horizontal mixing. This O$_3$ production contributes to a significant enhancement in annual mean O$_3$ over the Antarctic plateau (Helmig et al., 2007). While a weak coupling between stratospheric and tropospheric O$_3$ was inferred earlier (Oltmans and Komhyr, 1976), frequent stratospheric intrusions in this region were also reported (Cristofanelli et al., 2018; Das et al., 2020; Greenslade et al., 2017). There have been extensive studies on a range of species utilizing datasets from dedicated campaigns and projects over West Antarctica and South Pole (CHABLIS—Chemistry of the Antarctic Boundary Layer and the Interface with Snow, Jones et al., 2008; ISCAT—Investigation of Sulfur Chemistry in Antarctica, Davis et al., 2004; ANTCI—Antarctic Tropospheric Chemistry Investigation (Eisele et al., 2008); WAIS—West Antarctic Ice Sheet, Frey et al., 2005; Masclin et al., 2013). The variability of volatile organic compounds (VOCs), radicals, O$_3$ and its precursors has been investigated over the East Antarctic plateau and eastern coastal Antarctica (OPALE—Oxidant Production over Antarctic Land and its Export; Preunkert et al., 2012 and references therein). But the east coast of Antarctica remains a relatively less explored region as compared to west Antarctica and the South Pole.

The east coast of Antarctica is distinct from the west coast as well as the inland region of Antarctica. Relatively high levels of hydroxyl and peroxy radicals over eastern Antarctica (Dumont d'Urville; 66.67° S, 140.02° E, 40 m above mean sea level—amsl) during austral summer (Kukui et al., 2012) indicate chemical differences from west Antarctica (Palmer; 64.77° S; 64.05° W) where radical concentrations are lower. Short-term events of O$_3$ enhancements are observed over the coastal as well as inland regions with higher frequency during the summer season and they are associated with ultraviolet radiation reaching the surface, photochemical production and transport (Crawford et al., 2001; Frey et al., 2015; Cristofanelli et al., 2018; Legrand et al., 2016).

Net summertime O_3 production (4–5 nmol mol^{-1} d^{-1}) has been observed at the eastern coastal Antarctica through NO_x emission from snow (Legrand et al., 2009, 2016). In contrast, surface or boundary layer O_3 depletion are also observed mainly due to halogen chemistry involving iodine, bromine and chlorine oxides, being more frequent in west Antarctica (Saiz-Lopez et al., 2007; Simpson et al., 2007). Weaker or less frequent surface O_3 depletion is observed over the east coast compared to the west coast of Antarctica (Jones et al., 2013; Legrand et al., 2016).

Most studies of East Antarctica have been based on in situ measurements of various trace gases including radical species (O_3, NO, HONO, OH, DMS, BrO, etc.) at Dumont d'Urville, Syowa (69.00° S; 39.58° E, ~29 m amsl) and Zhongshan (69.37° S, 76.36° E, 18.5 m amsl; Kukui et al., 2012; Legrand et al., 2016, 2009; Murayama et al., 1992; Tian et al., 2022) stations. These studies have shown the surface O_3 variability on different scales (i.e., diurnal: ~2 nmol mol^{-1}, seasonal: ~18 nmol mol^{-1}, and long-term trend: 0.07±0.07 nmol mol^{-1} y^{-1}). Only few studies have analyzed the relevant larger-scale trace gas distributions and discussed the model performance of seasonal changes in surface O_3 or tropospheric O_3 (Wang et al., 2022; Griffiths et al., 2021), including halogen chemistry (Yang et al., 2005; Fernandez et al., 2019). Studies investigating the chemistry and dynamics of surface O_3 are scarce for Antarctica (Morgenstern et al., 2013). To the best of our knowledge, there are no comprehensive studies discussing the surface O_3 variability and associated processes based on the synergy of in situ measurements and chemistry-climate modeling over East Antarctica. It is timely to investigate the underlying processes since an increasing O_3 trend has been reported over this part of the world recently (Kumar et al., 2021).

Our study aims to contribute to the understanding of chemical and dynamical processes governing the surface O_3 variability over the east coast of Antarctica. We have conducted in-situ measurements during three different years and performed simulations using a global chemistry-climate model to unravel the atmospheric processes that control the summertime O_3 levels and variability. Details of the measurements and model simulations are given in the next section. Results of the O_3 variability and a comparison of model results with measurements, and an analysis of photochemical and dynamical contributions are presented in section 3. A summary, the main conclusions, and a future outlook are presented in section 4.

2 Measurements and model simulations

2.1 In situ measurements

Surface O_3 was measured at the Indian station Bharati (69.4° S, 76.2° E, ~35 m above mean sea level) at the Larsemann Hills in the east coast of Antarctica during the summer seasons of three years 2015–2017: 29 January–13 February 2015, 17 January–24 February 2016, and 11 December 2016–16 February 2017. The Bharati site experiences a surface pressure of ~980±10 hPa, cold temperatures (-0.1±3 °C; -11–8 °C), moderate humidity (60±13.5%; 34–98%) and mainly easterly winds with a number of blizzards during the summer season. A detailed overview of the meteorological conditions at Bharati station can be found in Soni et al., 2017.

Surface O_3 mixing ratios were measured using an online ultraviolet photometric ozone analyzer manufactured by the Environnement S.A, France (model O342). The instrument derives O_3 mixing ratios using the Beer–Lambert law considering the absorption of ultraviolet radiation around 253.7 nm by O_3 molecules. The measurement noise, lower detection limits, linearity and minimum response time are 0.5 nmol mol^{-1}, 1 nmol mol^{-1}, ±1 % and 10 s, respectively. The instrument was operated on the auto-response mode (response time of 10–90 s) under permissible range of temperature. O_3 mixing ratios were recorded continuously at 5 min averaging intervals. Air samples were drawn from a height of approximately 2 m above the ground level through a Teflon tube and filtered through 5 µm non-reactive polytetrafluoroethylene dust filter prior to injection into the analyzer. Prior to each expedition, the analyzer was calibrated for mixing ratios of 20 and 30 nmol mol^{-1} using a multichannel calibrator. The measurement uncertainty is estimated to be ~5 % (Tanimoto et al., 2007). In addition to measurements at Bharati, surface O_3 at Syowa and Arrival Heights (77.80° S; 166.67° E) available from https://ebas-data.nilu.no/Default.aspx for the study period are also used for the comparison of model results.

The vertical profiles of O_3 partial pressure were measured using balloon-borne electrochemical ozonesondes manufactured by the En-Sci Corporation, USA (Model: 2Z-V7). A total of 12 profiles were measured during the study period. The O_3 partial pressure was converted to O_3 mixing ratios using the simultaneously measured atmospheric pressure by radiosonde (model: iMet-1-RSB). Air is passed through an electrochemical concentration cell (ECC) using a built-in non-reactive pump, and the current generated by the electrochemical reaction of O_3 (with

potassium iodide) is measured by an electronic interface board and converted into an O_3 partial

pressure. The detailed operation principle and performance evaluation of ozonesonde instrument

are described in Komhyr et al., 1995 and references therein. The accuracy of O_3 measurements is

reported to be 5–10% up to an altitude of 30 km (Smit et al., 2007). Additional details of the O_3

measurements and meteorological parameters using this technique can be found elsewhere

(Ajayakumar et al., 2019; Ojha et al., 2014). Besides our measurements at Bharati, we utilized

available O_3 vertical profiles measured using ECC ozonesondes at Davis station (68.58° S 77.97°

E; https://data.aad.gov.au/metadata/records/AAS_4293_Ozonesonde) in this study.

The surface level wind speed and direction were measured using an automatic weather

station, which meets the standards of the World Meteorological Organization and was operated by

the India Meteorological Department. Wind direction measurements are used here to analyze the

changes in surface O_3 on a diurnal time scale. To understand the impacts of updraft and downdrafts,

the vertical wind at the surface was measured using a fast response ultrasonic anemometer (make:

METEK, GmBH, Germany; model: USA-1 Scientific). The factory calibrated sensor was mounted

at 3 m level above the ground and was operated at 25 Hz during January 2016. The measuring

resolution and accuracy of the vertical velocity are $\pm$ 0.01 m s^{-1} and 0.2 m s^{-1}, respectively. Further

details on the instrument can be found in (Reddy et al., (2021).

2.2   Model simulations

In this work the EMAC (ECHAM5/MESSy Atmospheric Chemistry) model (Jöckel et al.,

2010, 2006) has been used. This model is a numerical chemistry and climate simulation system

that includes sub-models describing tropospheric and middle atmospheric processes and their

interaction with oceans, land and human influences. It uses the second version of the Modular

Earth Submodel System (MESSy2) to link multi-institutional computer codes. The core

atmospheric model is the 5th generation European Centre Hamburg general circulation model

(ECHAM5, Roeckner et al., 2006). The physics subroutines of the original ECHAM code have

been modularized and reimplemented as MESSy submodels and have continuously been further

developed. Only the spectral transform core, the flux-form semi-Lagrangian large scale advection

scheme, and the nudging routines for Newtonian relaxation are remaining from ECHAM5. For the

present study we applied EMAC (MESSy version 2.55.0) in the T106L47MA-resolution, i.e. with

a spherical truncation of T106 (corresponding to a quadratic Gaussian grid of approximately 1.1° × 1.1° in latitude and longitude) with 47 vertical hybrid pressure levels up to 0.01 hPa. In this work we used the same set up as in Reifenberg et al. (2022), and the model results encompass the years 2014-2018 with a 3-hours output frequency. Global atmospheric chemistry models are known to overestimate tropospheric ozone (Young et al., 2018), and EMAC is no exception to this. Nevertheless, extensive ozone evaluation (Jöckel et al., 2016) shows that the EMAC model has a very low (less than 10%) or no bias in the troposphere against observations for latitudes below 60° S. Furthermore, the EMAC model has been extensively evaluated in the last years both for the gas phase (Jöckel et al., 2016; Taraborrelli et al., 2021) and for the aerosol phase (Pozzer et al., 2012; Brühl et al., 2018; Pozzer et al., 2022).

The model includes emissions of bromine from sea spray following the approach of Kerkweg et al. (2008), and important heterogeneous reactions involving bromine (e.g., liquid phase reactions of HOBr + HBr → Br$_2$ + H$_2$O) are included via the AERCHEM subroutines (Rosanka et al., 2023) in the GmXe submodel (Pringle et al., 2010). With the ONLEM submodel, the air-snow subroutine are activated (Falk and Sinnhuber, 2018), which include the bromine release on sea-ice and snow-covered surface, based on the scheme of Toyota et al. (2011). Beside the bromine release, no NO$_x$ release is included by the deposition of O$_3$. Note that NO$_x$ and HONO emissions from snowpack (Honrath et al., 2002; Bond et al., 2023) are not incorporated in the model.

To investigate the effects of transport, airmass back trajectories have been computed using the HYSPLIT (HYbrid Single Particle Lagrangian Integrated Trajectory) model version-4 (Rolph et al., 2017; Stein et al., 2015) with the input of 1°×1° gridded GDAS (Global Data Assimilation System) meteorological data.

3   Results and Discussions

3.1   O$_3$ variability: comparison of observations with model simulations

Figure 1a shows the elevation map of Antarctica marked with the location of the Indian station Bharati (69.4° S, 76.2° E, ~35 m amsl), where surface-based and balloon-borne measurements of O$_3$ have been conducted during this study. The surface elevation is higher (up to

4 km) over the eastern part of Antarctica. Figure 1b shows the spatial distribution of surface O_3 during summer of 2015–2017 (29 January–13 February 2015, 17 January–24 February 2016, and 11 December 2016–16 February 2017) as simulated by the EMAC model, along with the mean observed value at Bharati station (18.8 ± 2.3 nmol mol^{-1}). The mean O_3 distribution shows increase

215   from the oceanic region (10–16 nmol mol^{-1}) to the landmass (15–24~~3~~ nmol mol^{-1}), nearly following the topographical features of Antarctica. Overall, the model simulated spatial distribution of O_3 (Fig. 1b) is seen to be in agreement with the distribution based on measurements from different stations (Fig. S1). This is further consistent with previous studies showing higher O_3 mixing ratios over elevated site~~s~~ (~~Summit; 3212 m amsl and~~ South Pole; 2830 m amsl) as compared to the

220   coastal/oceanic region (Helmig et al., 2007). The balloon-borne observations (Fig. 3) also show increase in mean O_3 mixing ratios with altitude.

Figure 1c shows the stratospheric contribution (in percent) to the surface O_3 based on the stratospheric O_3 tracer in the model (O_3s). O_3s is seen to contribute by 4~~1~~0–5~~1~~0% over the Antarctic region with greater contribution (45–5~~1~~0%) over the continent with higher elevation than

225   that over the surrounding ocean (4~~1~~0–45%). The mean stratospheric contribution at the observation site Bharati is estimated to be ~47~~48~~% (~9~~10~~ nmol mol^{-1}), showing that nearly half of O_3 at the surface is of the stratospheric origin. Mihalikova and Kirkwood, 2013 have estimated a 6–7% occurrence rate of tropospheric folds (1-2 folds month^{-1}) during summer using radar observations at Troll station (72.0° S, 2.5° E, 1275 m amsl). In another recent study also, the enhancement by

230   20–30 nmol mol^{-1} (67–100% as compared to the climatological mean) is seen in upper tropospheric O_3 above Bharati station due to stratospheric intrusions (Das et al., 2020). In addition, gradual subsidence through the tropopause also contribute to stratospheric ozone transport into the troposphere. Therefore, stratospheric intrusions are suggested to transport the O_3-rich airmasses to the troposphere, which subsequently descend to the surface and get redistributed across the region

235   through horizontal transport. Descent of O_3-rich airmasses is further discussed in section 3.2.
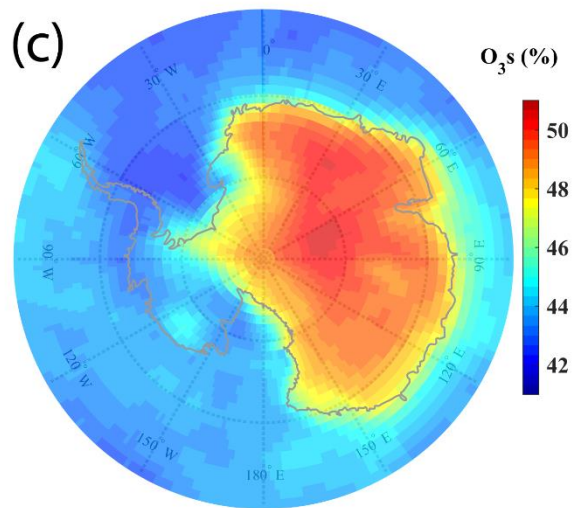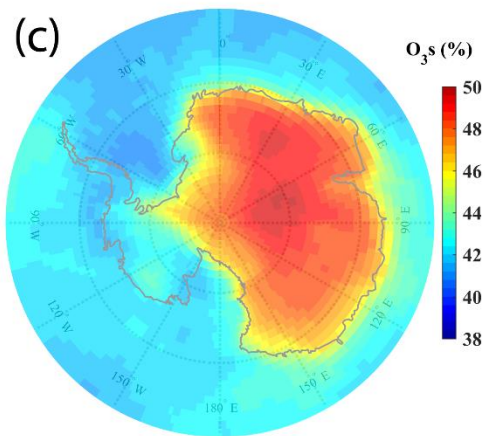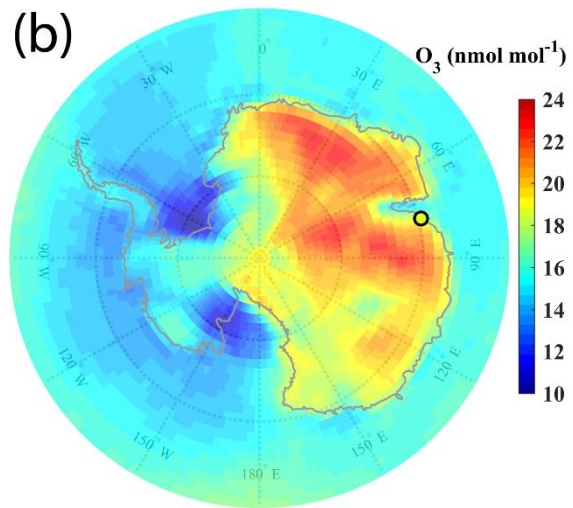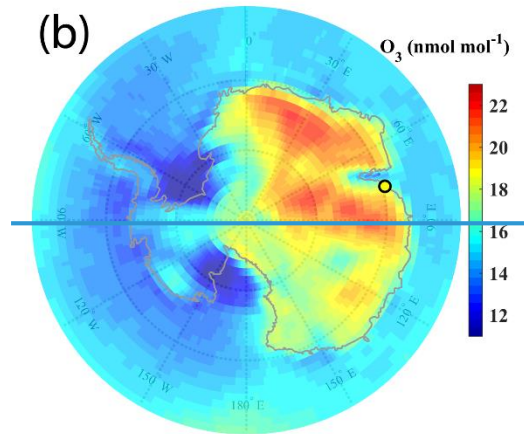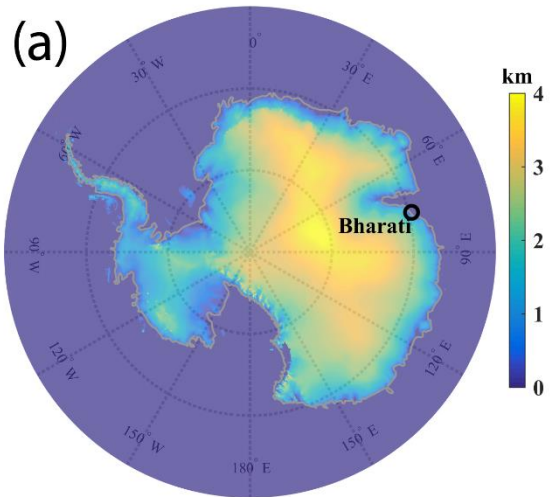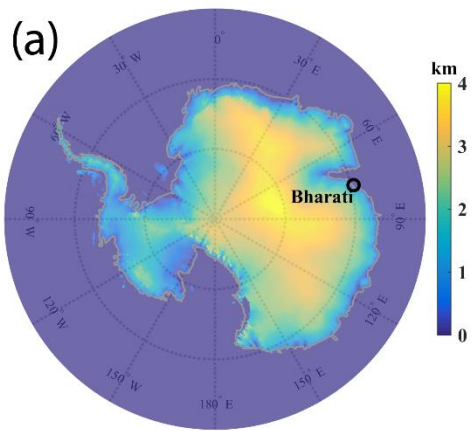
Figure 1. (a) Elevation map of Antarctica along with the location of the Indian station Bharati marked by a black circle. (b) Spatial distribution of surface O_3 simulated by the EMAC model, averaged over the study period (29 January–13 February 2015, 17 January–24 February 2016, and 11 December 2016–16 February 2017). Colour in the black circle in (b) represents the mean value from the in situ measurements at Bharati. (c) Percent contribution of stratospheric O_3 to the surface O_3 derived from the EMAC model during the study period.

240
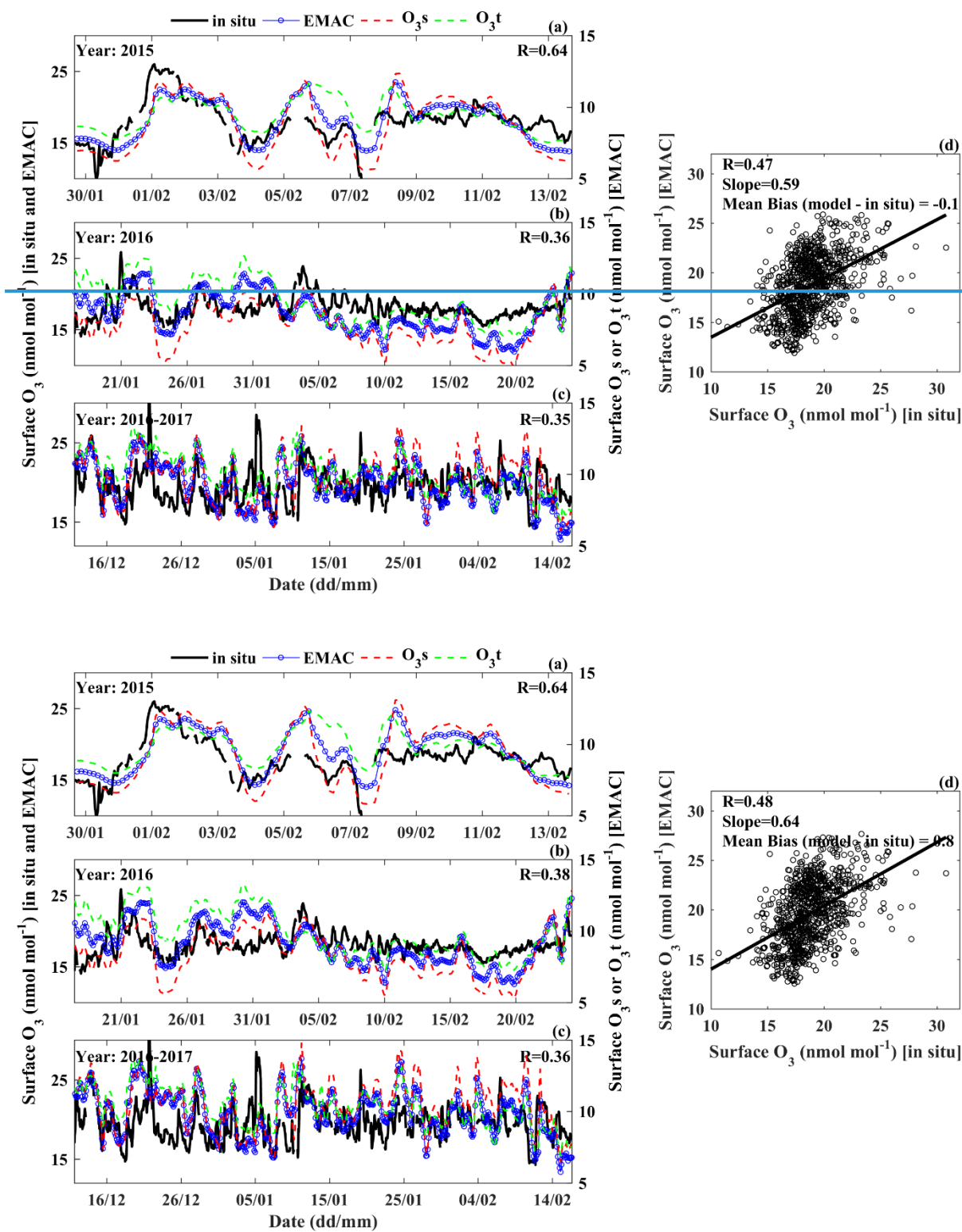
Figure 2. Variability in surface O$_3$ (a-c) at Bharati during austral summer of 2015–2017 based on in situ measurements (black) and EMAC simulations (blue). Green and red curves show the

absolute stratospheric (O$_3$s) and tropospheric (O$_3$t) contributions to the surface O$_3$. A scatter plot between in situ measurements and model simulated O$_3$ is shown in (d). Note that O$_3$s and O$_3$t are on a different scale on right-y axis in (a-c).

250   Figure 2a–c shows the variations in surface O$_3$ at Bharati station from in situ measurements and model simulations during the summer seasons of 2015–2017. The mean O$_3$ levels estimated from the model simulations (19.7 ± 3.2 nmol mol^{-1}) are in very good agreement with the measurements (18.8 ± 2.3) with negligible bias (~1 nmol mol^{-1}) at this station. Further, the surface O$_3$ level at Bharati is observed to be similar to an earlier observation (~13–20 nmol mol^{-1}) at this
255   station (Ali et al., 2017) and also to other stations in the coastal region of East Antarctica (Fig. S1). The model tends to successfully capture several features of the observed variability (Fig. 2a–c), nevertheless the overall correlation coefficient is 0.48 (Fig. 2d). The comparison for two other coastal stations, Syowa and Arrival Heights during the same study period also shows that the model can reproduce the summertime O$_3$ levels with small bias and the temporal variability moderately
260   well (Fig. S2–3). The blue and green curves in Fig. 2 show the individual contributions from stratospheric (O$_3$s) and tropospheric sources (O$_3$t=O$_3$ minus O$_3$s), respectively. Both stratospheric and tropospheric sources are estimated to be contributing nearly equally, 48% and 52%, respectively. Further, the stratospheric and tropospheric O$_3$ at the surface are seen to be strongly correlated (R=0.9; figure not shown) over most of the region mainly due to the mixing of
265   stratospheric and tropospheric airmasses during the transport from the tropopause to the surface. Direct transport of stratospheric air or ~~Strong~~ local O$_3$ production ~~(e.g., through NO$_x$ from snow) or direct transport of stratospheric air~~ would decrease the correlation or perturb the variations in O$_3$s and O$_3$t. Overall, similar variability of comparable magnitude in O$_3$s and O$_3$t indicate the absence of strong "local" production or "direct" stratospheric transport to the surface. However,
270   about 50% stratospheric contribution to surface O$_3$ points to significant stratospheric intrusions over the Antarctic region.
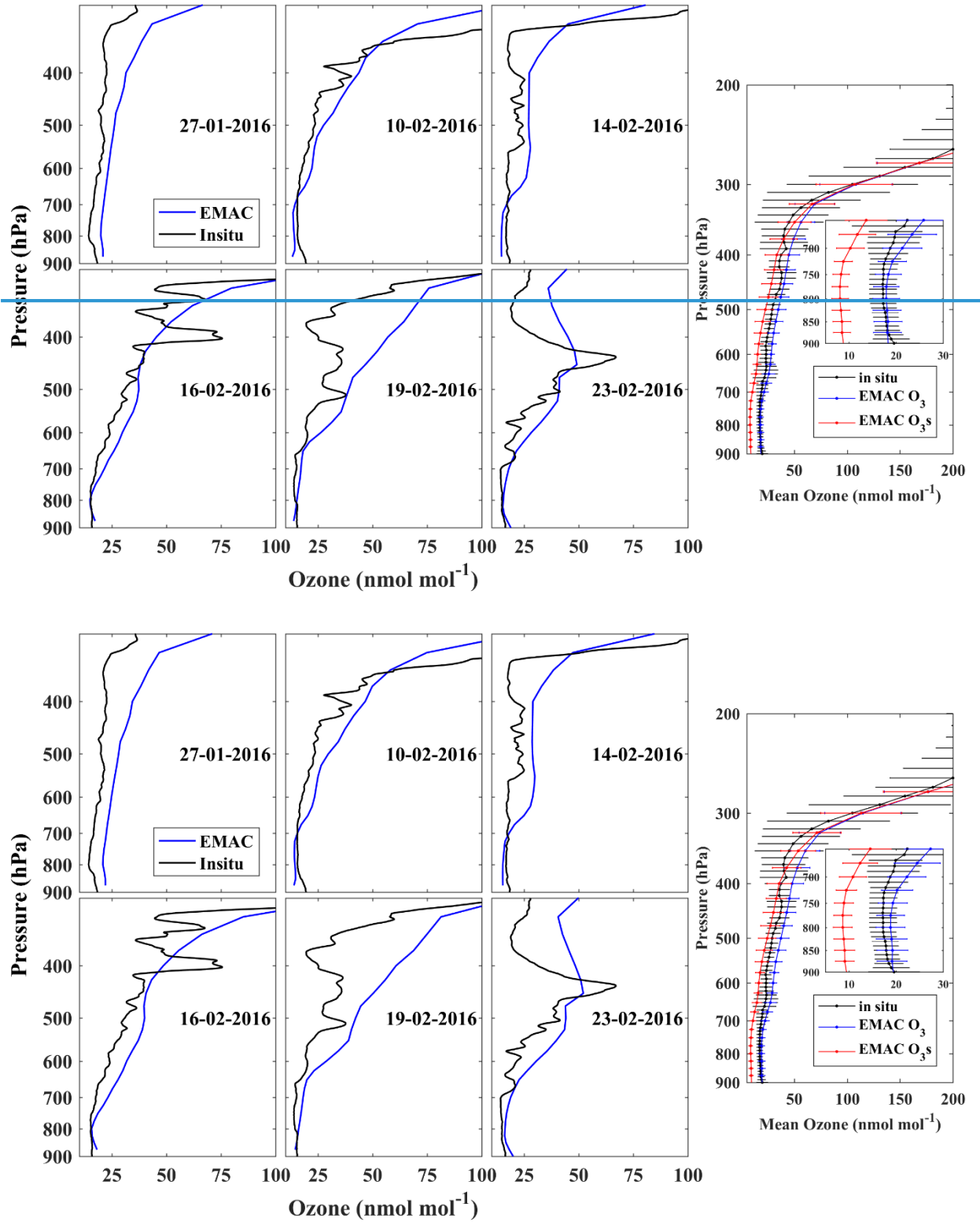
Figure 3. Vertical profiles of O₃ over Bharati station during a few representative days, based on

275 the in situ measurements (black) and EMAC simulation (blue). The insert on the right shows the mean vertical distribution of O_3 and O_3s (red) corresponding to 12 profiles during the study period.

Figure 3 shows the comparison of balloon-borne observations of O_3 vertical profiles with model simulation over Bharati station in 2016. Out of twelve, six individual representative profiles are shown in the figure. O_3 mixing ratios gradually increase with altitude up to the tropopause

280 (~8.5 km; ~300 hPa), showing also O_3 peaks in the middle/upper troposphere during some days. The model successfully captures the mean vertical distribution especially in the lower troposphere (pressure > ~700 hPa) with a mean bias of less than 2~~3~~ nmol mol^{-1}. There is an agreement between the model and observations in the upper troposphere, however, the model overestimates O_3 levels (by ~~~11~~ 12 nmol mol-1) at the tropopause. Ozonesonde measurements from another station in the

285 region, Davis (68.6° S, 78.0° E), were also compared with the model results for the study period (Fig. S4 and S5). The O_3 variability from model results (standard deviation: 3–13 nmol mol^{-1}) is comparable or slightly lower than the observed variability in the vertical distribution (950–350 hPa). The O_3s contribution is ~45–50% in the lower troposphere (pressure > ~700 hPa) but increases with altitude to 65% at 500 hPa up to 100% at and above the tropopause (~300 hPa). The

290 EMAC model captures both the mean vertical structure as well as some secondary O_3 peaks (e.g., 23 February 2016; Fig. 3) in the upper troposphere (~6 km; 450 hPa). However, there are some noticeable differences between model and observations on individual days (e.g., 19 February 2016; Fig. 3). The model limitation in reproducing some features of secondary peaks have been suggested to be due to coarser vertical resolution and the temporal differences (Ojha et al., 2017),

295 and confirmed recently in a study focusing on tropopause folding frequency (Bartusek et al., 2023).

Overall, the model reproduces the observed tropospheric O_3 distribution and most of the day-to-day variability in the surface and tropospheric O_3. It is to be noted that the performance of global chemistry-climate models is also limited by the parameterization schemes developed for such pristine environments with extreme climatic conditions (e.g., frequent blizzards). Note that

300 depletion of surface O_3 was observed over Antarctica during blizzards as blowing snow, which is a source of sea salt aerosols and subsequently bromine, could deplete O_3 (Jones et al., 2009; ~~(~~Ali et al., 2017). Nevertheless, our study fills a gap with respect to the evaluation of the widely applied EMAC model for the Antarctic region and the results may have implications to further improve the model in future studies.

305 **3.2 Influences of downward transport on surface O_3**

Several events of surface O_3 enhancements were observed during the study period, as illustrated in Fig. 2. Two such events on 23 February 2016 and 01 February 2015 are investigated in detail to understand the mechanism driving such variability.
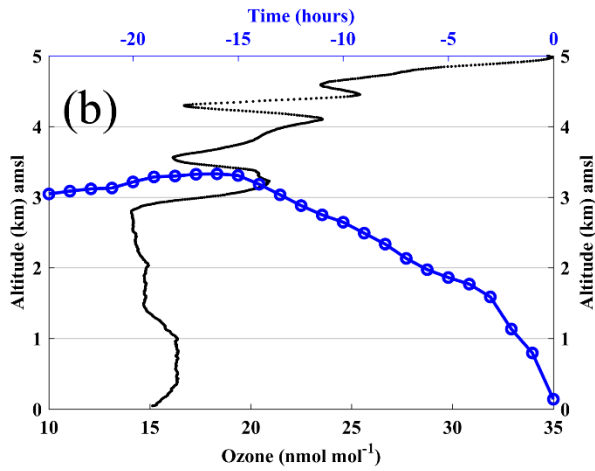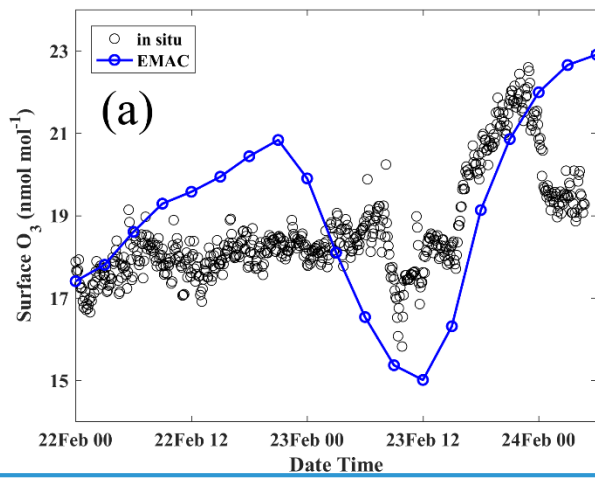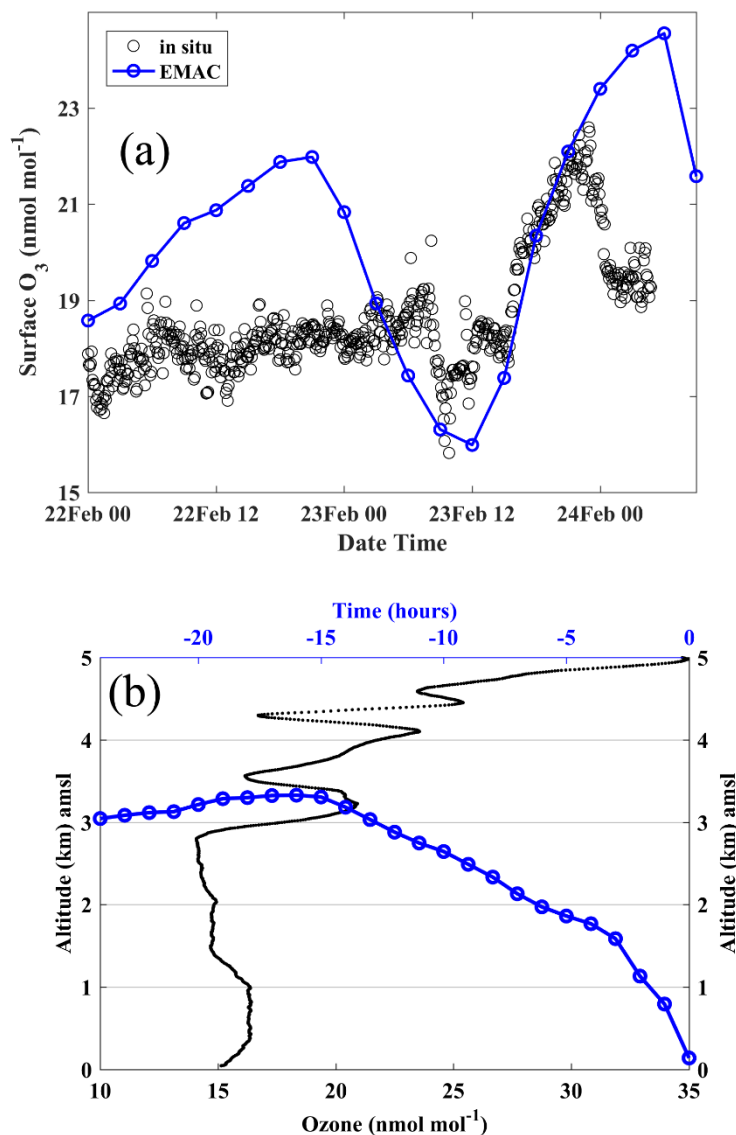
Figure 4. (a) ~~surface~~ Surface O$_3$ variations at Bharati station depicting an event of significant O$_3$ enhancement around 23:00 local time on 23 February 2016. (b) Variations in the altitude of airmass (blue) along the backward trajectory with respect to time from the O$_3$ enhancement event. Vertical profile of O$_3$ measured around 11:00 on 23 February 2016 (black).

Figure 4a shows that surface O$_3$ over Bharati was enhanced sharply by ~4 nmol mol^{-1} around 23:00 on 23 February 2016. Backward air mass trajectories show that this air mass originated from ~3 km altitude about 12 hours before the event. The balloon-borne O$_3$ vertical profile obtained at that time (11:00 on 23 February 2016; Fig. 4b) shows the presence of a layer with enhanced O$_3$ (~22 nmol mol^{-1}) relative to lower altitudes (~15 nmol mol^{-1}). Based on these collocated

320   observations and trajectory simulations, it is suggested that the O_3 rich air from this layer descended to the surface over Bharati in ~12 hours with a descent rate of >250 m h^{-1} (0.07 m s^{-1}). The estimated descent velocity seems to be consistent with the in situ measured mean vertical wind speed (0.09±0.29 m s^{-1}) measured at this station during 18–29 January 2016. The O_3 enhancement observed in the upper troposphere (~6 km; see Fig. 3) on 23 February 2016 is associated with a

325   stratospheric intrusion (Das et al., 2020). The presence of the jet-stream in the vicinity of the tropopause (~9 km altitude; ~300 hPa) can enhance the turbulence due to strong wind shear (squared wind shear=5 × 10^{-4} s^{-2}). Along with this turbulence, tropopause oscillations led to the stratospheric intrusion during 22–23 February 2016 (Das et al., 2020). The presence of similar surface O_3 enhancement events on several other days also (Fig. 2) suggests that this is a periodic

330   phenomenon that significantly contributes to tropospheric O_3 in the region.
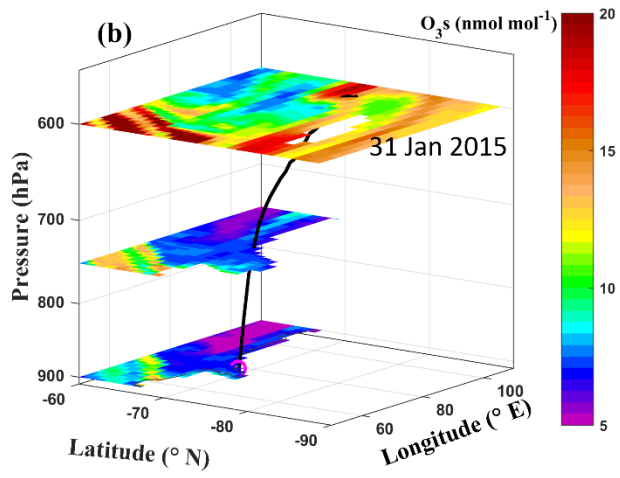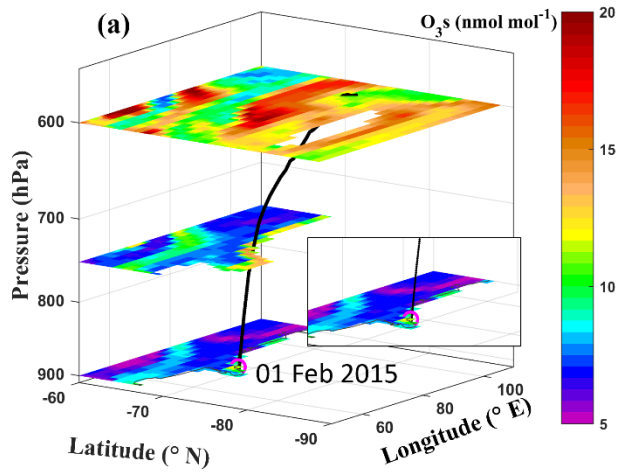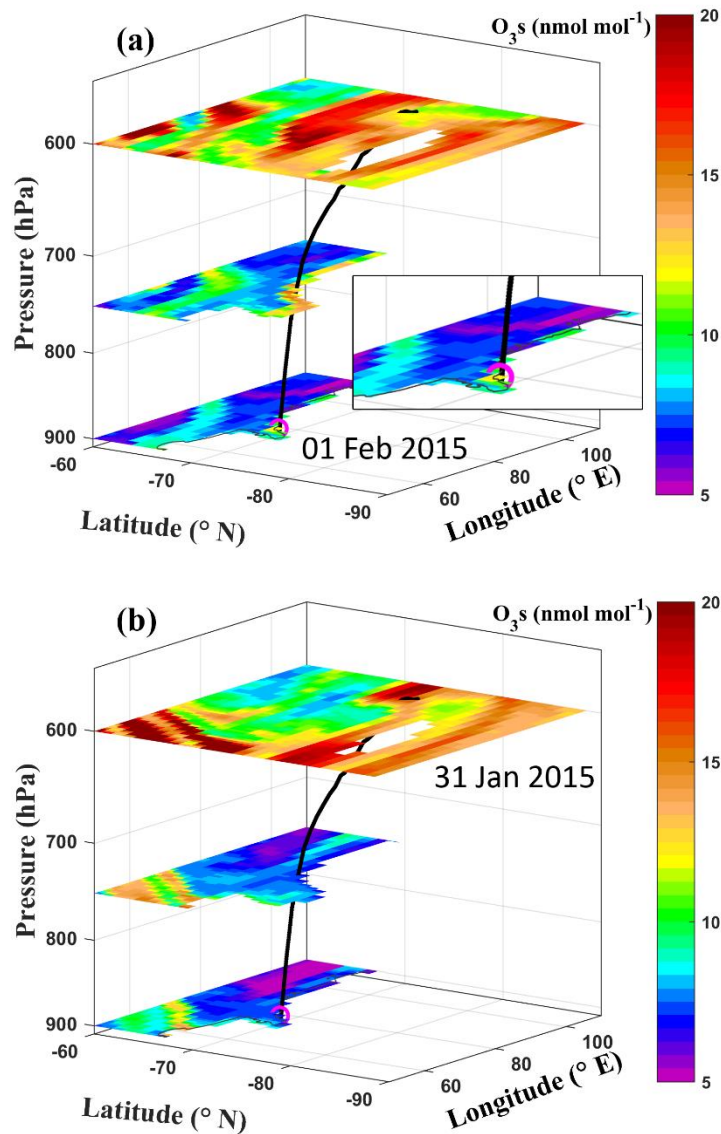
Figure 5. Spatial distribution of the stratospheric O_3 tracer in the model at different pressure levels for (a) 01 February 2015 depicting an enhancement at surface, and (b) 31 January 2015 depicting an enhancement in the upper troposphere. The black curve represents a 24-hour backward air mass trajectory ending at Bharati station (magenta circle) on 01 February 2015 and originating around 600 hPa on 31 January 2015.

Surface O_3 shows a continuous enhancement from about 12–14 nmol mol^{-1} on 31 January 2015 to about 25 nmol mol^{-1} on 01 February 2015 (Fig. 2a). To analyze the influence of transport from the stratosphere, the spatial distribution of the stratospheric O_3 tracer at different pressure levels is combined with airmass trajectories (Fig. 5). The insert in Fig. 5a shows a zoomed view

of O_3s around Bharati station on 01 February 2015. The airmass backward trajectory ending at Bharati station at the time of the observed enhancement is shown by the black curve. The airmass is traced back to ~600 hPa (~4 km) one day prior to the observed enhancement (i.e., 31 January 2015) at a lower latitude, where a patch of stratospheric O_3 (20 nmol mol^{-1}) is simulated by the model. A clear descent of airmass with a descent rate of ~0.05 m s^{-1} is seen, leading to the enhancement in surface O_3 on 01 February 2015.

The above analysis of two representative events shows that the intrusion of stratospheric O_3 followed by descent of O_3-rich air can cause a 4–10 nmol mol^{-1} enhancement in surface O_3 during the study period. The result is in line with a continuous increase in O_3 and O_3s with altitude, as shown in Fig. 1c and 3. Similar variations of O_3t compared to O_3s (Fig. 2) indicate significant air mass mixing during the transport process. O_3 enhancement events with similar magnitude were also observed at the nearby station Zhongshan (69.37° S 76.36° E; Ding et al., 2020; Tian et al., 2022) and with larger magnitude at South Pole (8–20 nmol mol^{-1}; Oltmans et al., 2008) attributed to transport or NO_x driven cumulative photochemical production, assuming a marginal role of transport from the stratosphere or free-troposphere (Cristofanelli et al., 2018; Ding et al., 2020). The occurrence of such O_3 enhancement is less evident over the coastal regions compared to the Antarctic plateau (Jones, 2003). However, substantial contributions of stratosphere-troposphere exchange were associated with airmass fluxes up to 60 kg m^{-2} d^{-1} (Sanak et al., 1985) using in situ measurement of Beryllium isotope at Dumont d'Urville station. Based on long-term balloon-borne measurements and GOES-Chem (Goddard Earth Observing System coupled with Chemistry) model simulations, Greenslade et al. (2017) also reported large stratosphere to troposphere O_3 fluxes (0.50–0.75 × 10^{17} molecules cm^{-2} month^{-1}) during summer, which exceed those during winter (0.25–0.50 × 10^{17} molecules cm^{-2} month^{-1}).

 ### 3.3   Influences of photochemistry on surface O₃
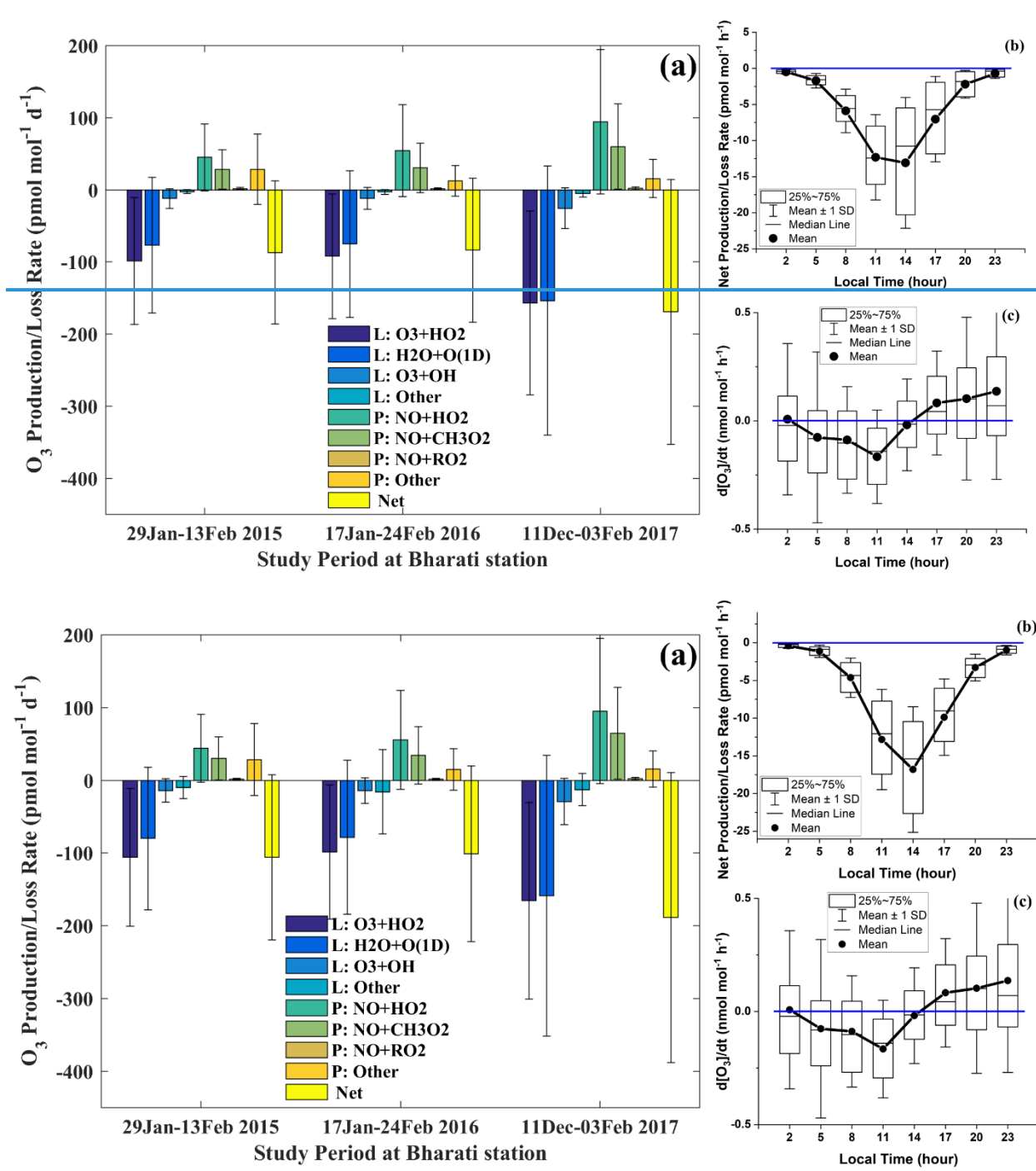
Figure 6. (a) Mean production and loss rates of surface O₃ through different chemical pathways at Bharati during the study period, (b) diurnal variation of net O₃ change due to photochemistry,

370   derived from the EMAC model simulations, and (c) rate of change of surface O_3 (dO_3/dt) based
        on the in situ measurements at Bharati station.

        The production and loss rates of O_3 through different chemical pathways have been
        estimated from the EMAC model simulation, and the mean values during the study period are
        shown in Fig. 6a. Among various production and loss reactions, O_3+HO_2 and H_2O+$O(^1D)$ are
375   found to be the dominant O_3 loss pathways, whereas NO+HO_2 and NO+CH_3O_2 are the major O_3
        production reactions. Overall, the aforementioned chemical losses tend to dominate the production
        leading to a net photochemical loss in surface O_3 at Bharati. Effectively the study region acts as a
        net chemical sink of O_3. Note that loss through O_3+OH and other reactions, and production through
        NO+RO_2 and other reactions are relatively small in magnitude (Fig. 6). Dry deposition over ice
380   and the surrounding ocean is a minor O_3 removal mechanism as well. The substantial variability
        (large error bars in Fig. 6a) in production and loss terms arises from the diurnal and day-to-day
        variations. Figure 6b-c shows the mean diurnal variation of net photochemical production or loss
        rates from the EMAC model and the rate of change of O_3 (i.e., dO_3/dt) from in situ measurements.
        The net loss is relatively high during noontime (11–14 h) and negligibly small after 23:00 and
385   prior to 5:00. In situ measured rate of change, dO_3/dt, is negative around 11:00 indicating overall
        loss which includes the influences of both photochemistry ~~as well as~~, dynamics and deposition
        losses. Since the mean amplitude of dO_3/dt in figure 6c is 0.3 nmol mol^{-1} h^{-1}, which is comparable
        or smaller than the variability at any given hour of the day, diurnal patterns on different days might
        vary from the mean picture. The positive rate of change after 17:00 and prior to 5:00 represents an
390   increase in O_3 mainly through horizontal or vertical transport as photochemistry is weak under
        conditions of low solar irradiance.

        Despite of being a net photochemical sink of surface O_3, it is observed that the levels of O_3
        are relatively steady or continuous over time (Fig. 2c). We estimated surface O_3 fluxes by
        multiplying the model simulated vertical wind with the O_3 concentration at the model level just
395   above the surface. Figure 7b shows the mean O_3 flux averaged over the study period. The negative
        flux represents the number of O_3 molecules moving downward (contributing to surface O_3) per
        unit area and per unit of time. A stronger downward flux along the east coast (Fig. 7b)
        counterbalances the net photochemical O_3 loss (Fig. 7a). Assuming a boundary layer height of 500
        m, the loss rates integrated over boundary layer are estimated at 2.7×10^{13} molecules m^{-2} s^{-1}, which

400 is of comparable magnitude to the modelled downward flux (Fig. 7b). O_3 and O_3 fluxes (~~mean of~~ fluxes at ~~surface and a~~ level just above the surface) correlate negatively (R=-0.3) at Bharati in the EMAC simulation, as shown in Fig. S6a. This is substantiated with a negative correlation of surface O_3 with the vertical wind (Fig. S6b), suggesting enhanced O_3 during conditions of descent. The results suggest that despite the net chemical sink of O_3, the surface O_3 is maintained by a flux

405 from above during the summer over the coastal region. The O_3 loss through chemistry is counterbalanced by the contribution from dynamics (or vice versa) over East Antarctica during austral summer.
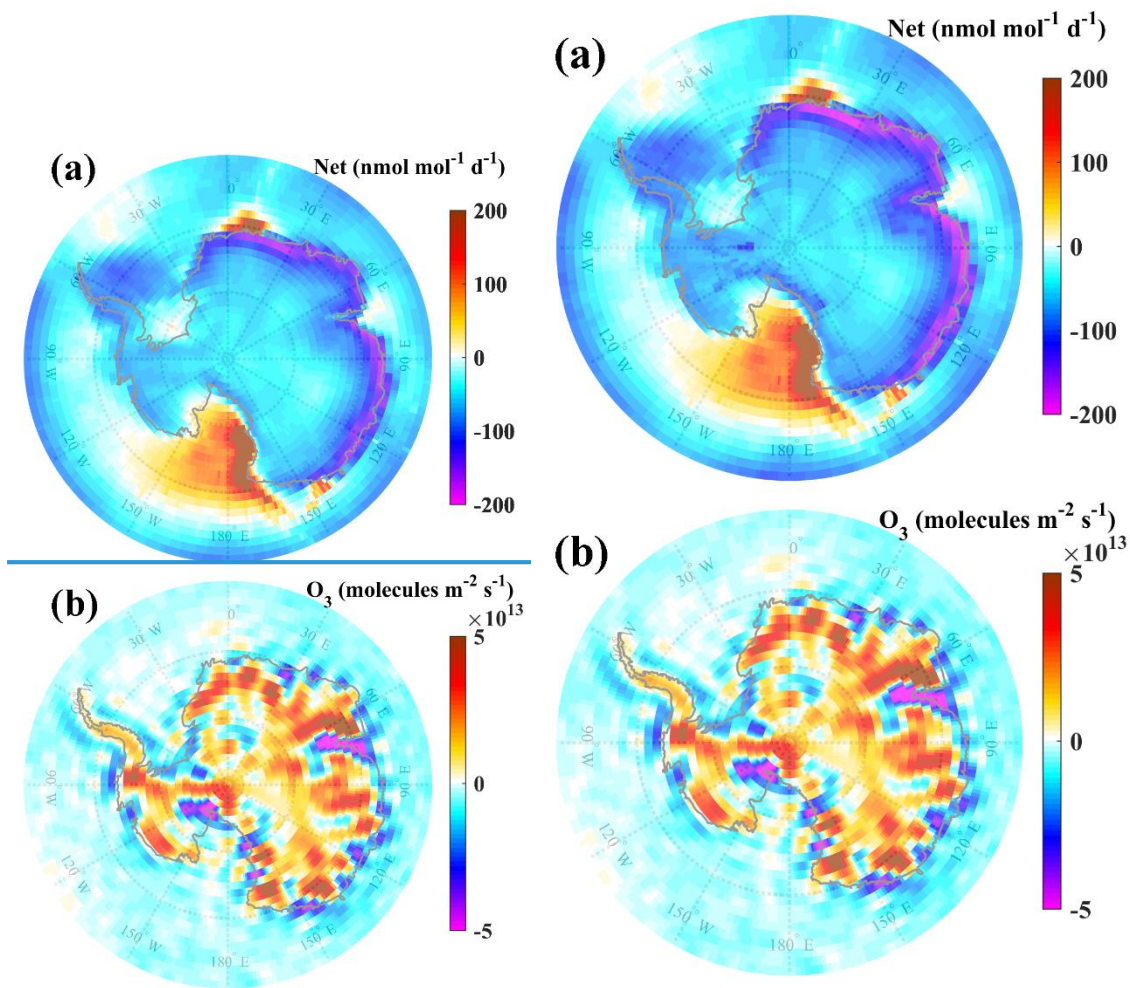
Figure 7. Spatial distribution of (a) net rate of change (production minus loss) of surface O_3 due
410 to photochemistry and (b) O_3 flux at surface averaged over the study period.

In order to understand whether the O_3 photochemical loss over the Bharati station also prevails over larger regions in Antarctica, we analyze the spatial distribution of net production or loss rates averaged during the austral summer (Fig. 7a). It is important to note that our simulations show that the entire Antarctic continent act as sink of O_3, in contrast to the previously reported net

415   O_3 production through NO emission from snow (Legrand et al., 2016 and references therein). In the east coastal Antarctic region O_3 loss rates are significantly higher (~190 pmol mol^{-1} d^{-1}) suggesting that it acts as a relatively strong chemical sink of surface O_3. The loss rate is at peak (~190 pmol mol^{-1} d^{-1}) over the east coast, higher by ~100 pmol mol^{-1} d^{-1} compared to adjacent land and ocean, and it gets further lower (~50 pmol mol^{-1} d^{-1}) much away from the coast. Note that

420   model simulated mean OH and NO are in the range of 0.05–0.5×10^6 molecules cm^{-3} and 0.5–10 pmol mol^{-1}, respectively, over entire the Antarctic region which is in line with earlier measurements at the west coast (OH mean: 0.11×10^6 molecules cm^{-3}, ranging <0.1–0.9×10^6 molecules cm^{-3}; NO: estimated value of 5 pmol mol^{-1}) by Jefferson et al., 1998 and Bloss et al., 2010, but lower (almost 5 times) than those measured during OPALE campaign (OH mean: $2.1 \times$

425   10^6 molecules cm^{-3}, ranging <0.8–6.2×10^6 molecules cm^{-3}; NO: 5–70 pmol mol^{-1}; Kukui et al., 2012).
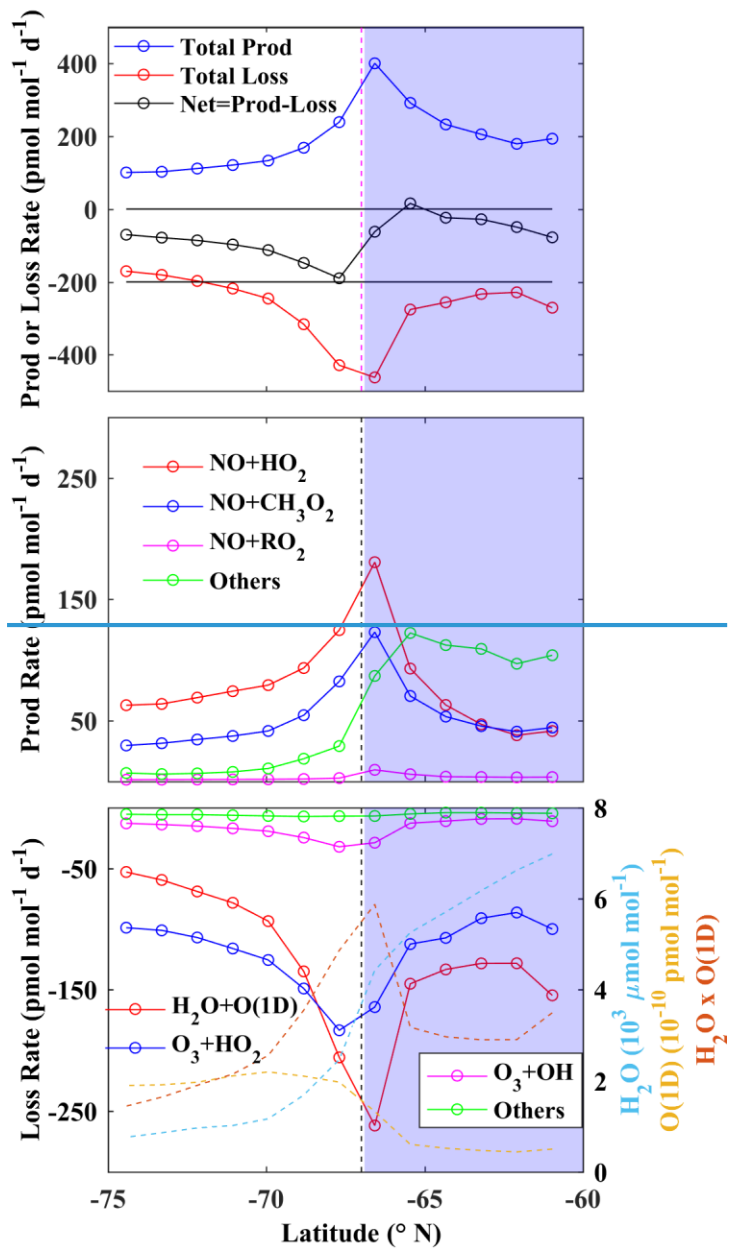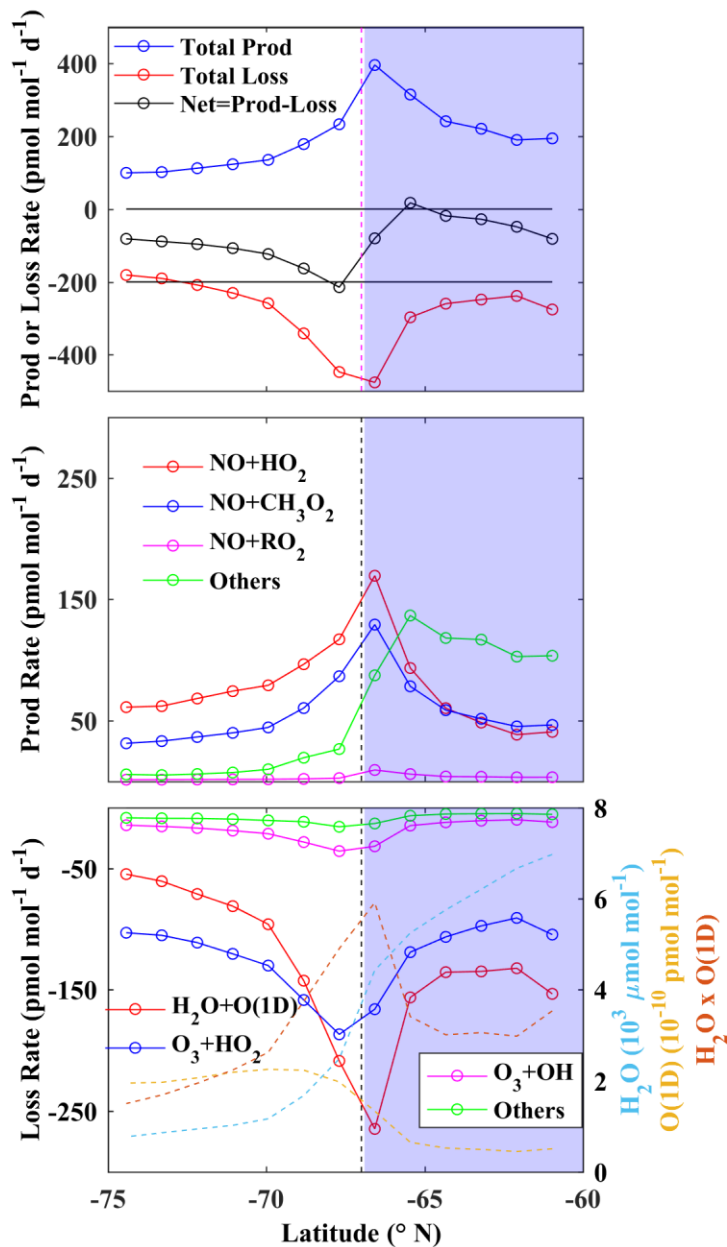
Figure 8. Latitudinal variation of production, loss and net rates of changes of surface O_3 averaged along the east coastal longitudinal band of 15–130° E during January 2017. The blue areas represent the ocean environment and vertical dashed line shows the approximate coast line.

The net O_3 loss rate (Fig. 7a) is found to be lower over land than over ocean and is highest along the east coast. We further considered 6 grids at both sides of the coast line and averaged over the longitude range 15–130° E (i.e., East Antarctica). The variations in average production, loss and net rates with latitude are shown in Fig. 8. Since the latitude corresponding to different grids

at 15–130° E are different, latitudes shown on the x-axis represent average latitudes. Thus, as we proceed from left to right (lower latitude to higher latitude) in Fig. 8, we move from land to ocean.

From Fig. 8a, it is clearly seen that the O_3 production as well as loss are maximum near the coast. Since loss dominates over the production, the net rate is negative with ~190 pmol mol^{-1} d^{-1}. Figure 8b and c represent changes in different production and loss pathways across the coast. The photolytic O_3 loss, followed by $H_2O+O(^1D)$, is found to be the dominating loss process peaking at ~300 pmol mol^{-1} d^{-1} along the coast. The reason for the peak loss rate at coast is related to the opposite latitudinal gradients in H_2O and $O(^1D)$ (see Fig. 8c; right axis). H_2O is substantially higher (~6000 μmol mol^{-1}) over ocean but much lower (1000 μmol mol^{-1}) in the drier atmosphere above continent. In contrast, $O(^1D)$ is higher (2×10^{-10} pmol mol^{-1}) over the continent primarily due to intense solar insolation at higher elevation and over the bright ice surface. Therefore, latitudinally opposite variations of H_2O and $O(^1D)$ lead to a relative maximum in $H_2O+O(^1D)$ near the coast. We also note that there is significant O_3 production over the ocean due to reactions other than the three primary reactions of peroxy radicals (HO_2, RO_2, CH_3O_2) with NO.

Thus, Uunder the prevailing relatively strong O_3 sink along the east coast, the mean O_3 level during summer is maintained by the downward flux of O_3 from the stratosphere.

3.4 Diurnal variation of surface O_3 at Bharati

Considering day-to-day variability, including enhancement events governed by stratospheric influence, ΔO_3 is computed by subtracting the running mean O_3 (288 points; 5 min interval—daily running mean) from the observed O_3. Figure 9a shows the mean diurnal variation of ΔO_3 during the 18 January–23 February 2016 period for which measurements of horizontal wind at surface were also available. Surface O_3 exhibits a diurnal variation, being relatively low during the afternoon (15:00 local time) and relatively high during nighttime (Fig. 9) with a diurnal amplitude of ~1.2 nmol mol^{-1}. Figure 9b shows the wind rose color coded with ΔO_3 mixing ratios. Sunlight at Bharati is abundant during summer and the land-sea thermal contrast explains the typical diurnal change in the wind direction under normal meteorological conditions, i.e., excluding blizzards and snow storms. Figure S7 shows time series of the wind direction and surface ΔO_3, depicting the link between O_3 and the wind direction. Due to higher O_3 over the eastern Antarctic land regions, winds from that sector transport the O_3-rich air to the Bharati station causing enhanced O_3 mixing

465 ratios. O_3 is higher when wind is parallel to the coast (easterly; wind direction ~90°) or from the land (wind direction: 90–240°). Under calm wind condition, the influence of transport is minimal and photochemical loss is more pronounced. When the wind is weak and from the ocean (wind direction: 30–90° N), O_3 levels are lower due to dilution by mixing with air from the oceanic sector. The O_3 diurnal variation is also closely linked with the vertical wind. Based on limited in

470 situ measurements of the vertical wind at the surface during 18–29 January 2016, the mean diurnal variation of vertical wind (w) along with ΔO_3 is shown in Fig. 9c. Downdrafts and stronger updrafts (up to ~0.4 ms^{-1}) are seen during nighttime (or lower solar zenith angle; 20:00–07:00) and daytime (08:00–19:00), respectively. Higher O_3 during nighttime is associated with downdrafts and O_3 mixing ratios are reduced with increasing updraft intensity. The EMAC model shows

475 limitations in reproducing the observed diurnal variation likely because of coarse resolution averaging out the topography and mesoscale dynamics.
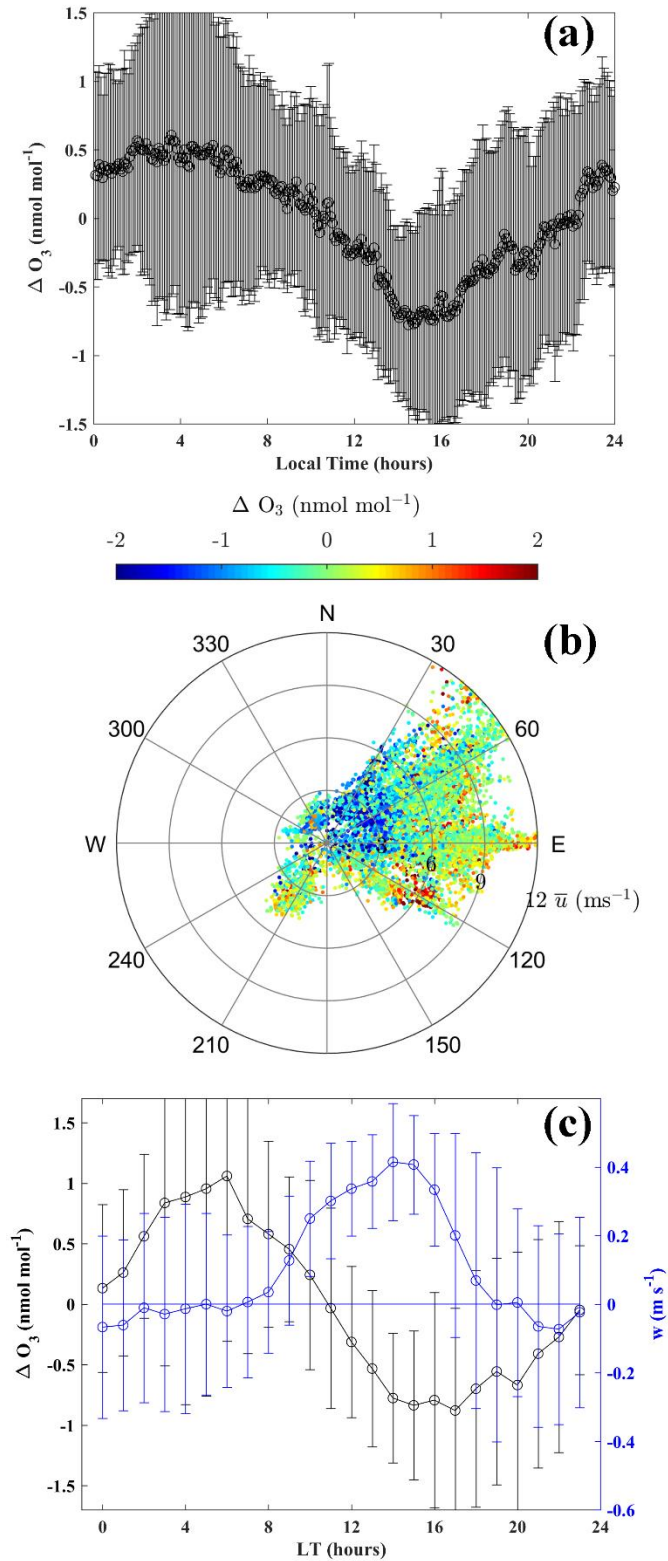
Figure 9. (a) Diurnal variation of ΔO_3, (b) wind rose color coded with ΔO_3, and (c) variation in collocated vertical wind and ΔO_3 at Bharati during the austral summer of 2016.

Diurnal patterns with an amplitude ranging from ~0.2–2 nmol mol^{-1} were reported at coastal (Syowa and McMurdo) and inland (Concordia; (75° S; 123° E; 3220 m above sea level) stations (Ghude et al., 2006; Legrand et al., 2009). However, such a pattern is absent over the South Pole (Oltmans, 1981). Interestingly, photochemical production during the morning hours (05:00–11:00)

485 due to the NO$_x$ released from snow was followed by a reduction due to an increase in boundary layer height (200 ±100 m) at the inland station Concordia (Legrand et al., 2009; 2016). Shallow convective boundary layers (less than 300 m) were reported over the Antarctic Plateau region by Mastrantonio et al. (1999). Unlike these studies, we did not observe photochemical O$_3$ production nor a clear signature of changes in O$_3$ transport across the top of boundary layer from our

490 ozonesonde measured O$_3$ profiles over Bharati station. Therefore, the diurnal patterns of O$_3$ over coastal Antarctica are found to be different than those over the inland region, mainly due to differences in meteorological conditions and the concentrations of precursor gases.

3.5 Absence of signature of halogen chemistry

Reactive halogens (e.g., iodine, bromine) have been shown to deplete O$_3$ in the boundary

495 layer over the Antarctic region (Barrie et al., 1988; Oltmans and Komhyr, 1976). However, ground-based remote sensing observations found very low concentrations of iodine oxide (~0.3±0.1 pmol mol^{-1}) in the boundary layer over Bharati station during the study period (Mahajan et al., 2021) and no clear sign of O$_3$ depletion was observed.

Satellite (SCIAMACHY—SCanning Imaging Absorption spectroMeter for Atmospheric

500 CartograpHY and OMI—Ozone Monitoring Instrument) observations also show lower monthly mean iodine monoxide (IO) columnar density (0–1×10^{12} molecules cm^{-2}) over Bharati compared to west Antarctica (figure not shown). This is consistent with previous studies (e.g., Schönhardt et al., 2012) showing relatively low IO over east Antarctica and the adjacent ocean (≤0.7 × 10^{12} molecules cm^{-2}) compared to west Antarctica (~1.5 × 10^{12} molecules cm^{-2}) during summer season

505 (December-January-February 2004–2009).

Bromine (Br) driven O$_3$ depletion events, resulting into BrO, are less frequent over the Antarctic region compared to the Arctic region due to differences in springtime surface temperatures (Tarasick and Bottenheim, 2002). However, large O$_3$ depletion events were observed

at Neumayer (70.62° S, 8.37° W; 42 m amsl) during the late winter (July to September), likely due to stronger BrO episodes from the larger sea ice coverage around the site (Legrand et al., 2009). Analysis of BrO from OMI possibly indicates an O_3 depletion event on 7 February 2015 at Bharati where BrO was enhanced, ~9.2×10^{13} molecules cm^{-2} with lower O_3 (~7 nmol mol^{-1}), marked by red rectangle in Fig. S8. Except for this event, BrO remained below 8×10^{13} molecules cm^{-2} around Bharati station (±0.5° latitude/longitude) during the study. O_3 depletion was also not seen at Syowa (Fig. S9) during the study period. The coastal region of east Antarctica exhibits slightly higher values of BrO (~7×10^{13} molecules cm^{-2}) compared to the ocean and land regions ($4–6 \times 10^{13}$ molecules cm^{-2}). However, it is low ($4–8 \times 10^{13}$ molecules cm^{-2}) during December–February (2004–2009) compared to the levels during September–November ($5–10 \times 10^{13}$ molecules cm^{-2}) over the Antarctic region (Schönhardt et al., 2012). The impact of Br chemistry on surface O_3 is suggested to be weaker along the east coast of Antarctica (Dumont d'Urville and Syowa) in contrast to western coastal Antarctica as observed over the Neumayer and Halley (75.55° S, 26.53° W, 30 m amsl) stations (Legrand et al., 2016). Nevertheless, simultaneous measurements of O_3 and halogen species including BrO are desirable to quantify the role of halogen chemistry over eastern Antarctica.

3.6   Surface O$_3$ during winter

To take into account the seasonality of O_3 at the surface, the wintertime distribution is shown in Fig. S10. Mean surface O_3 level is higher during winter (20–32 nmol mol^{-1}) compared to the summer (11–23 nmol mol^{-1}), in line with the reported seasonality in the literature (Legrand et al., 2009). Figure S10 reveals three low-O_3 patches over the coastal oceanic region. One is close to Bharati station, however, we do not have observations during wintertime for comparison. Model simulations suggest that surface O_3 is composed of 63–67% O_3s of stratospheric origin during winter (Fig. S10b), which is significantly higher than during austral summer. The probability of downward transport from the stratosphere during winter, also associated with a lower altitude of the tropopause, is larger (Kumar et al., 2021). Comparison of surface O_3 at Syowa (69.00 °S; 39.58 °E; not shown here) shows that the model captures the variability with R=0.3 and a negative bias of ~5 nmol mol^{-1}. The model performance seems to be better during summer, indicative of limitations to reproduce the mean O_3 concentrations and the variability during winter. Further studies are needed to understand and rectify the factors causing greater bias in the model during

winter. Analysis of the O_3 budget suggests a small net loss of O_3 by 10–25 pmol mol^{-1} d^{-1} over the oceanic region and close to zero (<5 pmol mol^{-1} d^{-1}) over the Antarctic continent (Fig. S11). To study this in greater detail, we highly recommend to conduct continuous wintertime measurements of O_3, its precursors including halogens over Bharati during winter season.

4   Summary

Ground- and balloon-borne O_3 measurements have been conducted over the Indian station Bharati at the east coast of Antarctica during the austral summers of 2015–2017. The observations have been used to evaluate the performance of the global chemistry-climate model EMAC over this part of the world. A comprehensive analysis of observations and model simulations provided significant insights into the dynamical and photochemical processes affecting surface O_3 and its variability. The main results are:

1. Surface O_3 levels over the Indian station Bharati at the eastern coastal Antarctica have been observed to be ~19 nmol mol^{-1} with a small variability of ~2 nmol mol^{-1} during austral summer. While similar levels prevail over the east coast, O_3 is typically higher over land at higher elevation. EMAC model successfully reproduced the observed mean levels with negligible bias over this unique environment and also captured the temporal variability (R=0.5). In particular, the model successfully reproduced some events during which O_3 was enhanced. Analysis of the stratospheric O_3 tracer in the model suggests that 41̶0̶–51̶0̶% of surface O_3 is of stratospheric origin with larger fractions over the higher elevation regions in Antarctica.

2. The model successfully reproduced the mean vertical distribution of O_3 over Bharati observed by balloon-borne soundings. Detailed analysis combining the balloon profiles, model tracers, and air mass trajectories shows that downward transport caused the observed events during which O_3 was enhanced.

3. Along the east coast of Antarctica, including Bharati station, photochemistry acts as a relatively strong sink of surface O_3 (~190 pmol mol^{-1} d^{-1}) when compared to adjacent land and ocean regions. Chemical loss through O_3 photolysis (followed by $H_2O+O(^1D)$)) and O_3+HO_2 dominates over the major production (through $NO+HO_2$ and $NO+CH_3O_2$). Reverse latitudinal gradients between H_2O and $O(^1D)$ lead to maximum O_3 loss at the coastal region. The continuous chemical loss is found to be counterbalanced by downward O_3 transport from above. The findings show the intertwined roles of dynamics and photochemistry that govern the O_3

variability over east Antarctica, and maintaining significant O_3 levels despite the absence of
570   local precursor sources.

4. In addition to the role of photochemistry, the diurnal variation of O_3 at Bharati was found to correlate with the diurnal wind changes. Surface O_3 varied with a diurnal amplitude of 1.2 nmol mol^{-1}, with the higher levels occurring when the wind blew parallel to the coast or from land regions. In addition, up- and downdrafts also play a role in the diurnal variation.

575

Our observations during austral summer over three years complement available data e.g. from eastern coastal Antarctica. The observations, besides revealing diurnal and day-to-day variability, helped in evaluating the performance of a global chemistry-climate model over this unique, pristine environment. The study provides valuable insights into the complementary roles
580   of photochemistry and dynamics in governing O_3 and its variability over Antarctica. In view of increasing anthropogenic activities and the changing climate, monitoring of O_3 and related species (NO, NO_2, CO, VOCs and halogens) is needed.

585   *Code availability.* The Modular Earth Submodel System (MESSy) is continuously further developed and applied by a consortium of institutions. The usage of MESSy and access to the source code is licensed to all affiliates of institutions that are members of the MESSy Consortium. Institutions can become a member of the MESSy Consortium by signing the MESSy Memorandum of Understanding. More information can be found on the MESSy Consortium Website
590   (http://www.messy-interface.org, last access: 04 July 2023). The code presented here has been based on MESSy version 2.55 and is available as git commit #a5bd54d5b in the MESSy repository.

Data availability. Measured ozone and EMAC simulated fields shown in the figures can be obtained from the website of Space Physics Laboratory (https://spl.gov.in/SPLv2/index.php/spl-
595   metadata/104-spl/550-trace-gases-metadata.html) or from the direct link, https://spl.gov.in/SPLv2/images/SPL-METADATA/Girach_et_al_2024_ACP_Ozone_Bharati_Antarctica.xlsx~~https://spl.gov.in/SPL/images/SPL-METADATA/Ozone_Bharati_Antarctica_Summer_2015-2017.xlsx~~.

Author contributions. I.A. Girach conceptualized and designed the study, performed measurements and analysed the datasets. K.V. Subrahmanyam, Koushik N., Mohammed Nazeer M., N.V.P. Kiran Kumar contributed in the measurements. A. Pozzer preformed the model simulations. N. Ojha, A. Pozzer, P.R. Nair, S.S. Babu and J. Lelieveld helped I. A. Girach in the analysis and interpretation of the results. I. A. Girach wrote the manuscript and all the co-authors contributed to the review and editing.

Declaration of competing interest. At least one of the (co-)authors is a member of the editorial board of Atmospheric Chemistry and Physics.

Acknowledgements. We gratefully acknowledge the organiser, Centre for Polar and Ocean Research (NCPOR), Goa, Ministry of Earth Sciences, India for providing the opportunity to participate in the 34th, 35th and 36th Indian Scientific Expedition to Antarctica (ISEA). We also acknowledge the leaders of Bharati Station and Voyage for providing necessary support for the smooth conduct of experiments at Bharati station. We are really thankful to Mr. Santosh Muralidharan, Space Physics Laboratory; Mr. Brijesh Desai, Laboratory in-charge of Bharati station during 35th expedition and other expedition members of 34th, 35th and 36th ISEA for their help during the field measurements. We are also thankful to India Meteorological Department (IMD) for providing meteorological observations, hydrogen gas cylinders for balloon ascents and for the help during balloon launches. The EMAC model simulations have been performed at the German Climate Computing Centre (DKRZ). Surface ozone observations at Antarctic stations (South Pole, United States; Arrival Heights, New Zealand; Marambio, Argentina; Syowa, Japan) were obtained from the newly established World Data Centre for Reactive Gases (WDCRG), WMO's GAW (Global Atmosphere Watch; World Meteorological Organization) programme (https://ebas.nilu.no/ and https://ebas-data.nilu.no/Default.aspx). Vertical O_3 profiles measured at Davis station were obtained from https://woudc.org/data/explore.php. We highly acknowledge teams of researchers who made ozone measurements at various Antarctic stations and made them available publically. We also acknowledge the NOAA Air Resources Laboratory (ARL) for providing air mass trajectory from the HYSPLIT transport and dispersion model from their READY website (http://www.arl.noaa.gov/ready.php).

630

References

Ali, K., Trivedi, D. K., and Sahu, S. K.: Surface ozone characterization at Larsemann Hills and Maitri, Antarctica, Sci. Total Environ., 584–585, 1130–1137,

635   https://doi.org/10.1016/j.scitotenv.2017.01.173, 2017.

Barrie, L. A., Bottenheim, J. W., Schnell, R. C., Crutzen, P. J., and Rasmussen, R. A.: Ozone destruction and photochemical reactions at polar sunrise in the lower Arctic atmosphere, Nature, 334, 138–141, https://doi.org/10.1038/334138a0, 1988.

Bartusek, S., Wu, Y., Ting, M., Zheng, C., Fiore, A., Sprenger, M., and Flemming, J.: Higher-

640   Resolution Tropopause Folding Accounts for More Stratospheric Ozone Intrusions, Geophys. Res. Lett., 50, e2022GL101690, https://doi.org/10.1029/2022GL101690, 2023.

Bloss, W. J., Camredon, M., Lee, J. D., Heard, D. E., Plane, J. M. C., Saiz-Lopez, A., J.-B. Bauguitte, S., Salmon, R. A., and Jones, A. E.: Coupling of HOx, NOx and halogen chemistry in the antarctic boundary layer, Atmos. Chem. Phys., 10, 10187–10209,

645   https://doi.org/10.5194/acp-10-10187-2010, 2010.

Bond, A. M. H., Frey, M. M., Kaiser, J., Kleffmann, J., Jones, A. E., and Squires, F. A.: Snowpack nitrate photolysis drives the summertime atmospheric nitrous acid (HONO) budget in coastal Antarctica, Atmos. Chem. Phys., 23, 5533–5550, https://doi.org/10.5194/acp-23-5533-2023, 2023.

650   Brühl, C., Schallock, J., Klingmüller, K., Robert, C., Bingen, C., Clarisse, L., Heckel, A., North, P., and Rieger, L.: Stratospheric aerosol radiative forcing simulated by the chemistry climate model EMAC using Aerosol CCI satellite data, Atmos. Chem. Phys., 18, 12845–12857, https://doi.org/10.5194/acp-18-12845-2018, 2018.

Crawford, J. H., Davis, D. D., Chen, G., Buhr, M., Oltmans, S., Weller, R., Mauldin, L., Eisele,

655   F., Shetter, R., Lefer, B., Arimoto, R., and Hogan, A.: Evidence for photochemical production of ozone at the South Pole surface, Geophys. Res. Lett., 28, 3641–3644,

https://doi.org/10.1029/2001GL013055, 2001.

Cristofanelli, P., Putero, D., Bonasoni, P., Busetto, M., Calzolari, F., Camporeale, G., Grigioni, P., Lupi, A., Petkov, B., Traversi, R., Udisti, R., and Vitale, V.: Analysis of multi-year near-surface ozone observations at the WMO/GAW "Concordia" station (75°06′S, 123°20′E, 3280 m a.s.l. – Antarctica), Atmos. Environ., 177, 54–63, https://doi.org/10.1016/j.atmosenv.2018.01.007, 2018.

Das, S. S., Ramkumar, G., Koushik, N., Murphy, D. J., Girach, I. A., Suneeth, K. V., Subrahmanyam, K. V., Soni, V. K., Kumar, V., and Nazeer, M.: Multiplatform observations of stratosphere-troposphere exchange over the Bharati (69.41° S, 76° E), Antarctica during ISEA-35, J. Atmos. Solar-Terrestrial Phys., 211, https://doi.org/10.1016/j.jastp.2020.105455, 2020.

Davis, D. D., Eisele, F., Chen, G., Crawford, J., Huey, G., Tanner, D., Slusher, D., Mauldin, L., Oncley, S., Lenschow, D., Semmer, S., Shetter, R., Lefer, B., Arimoto, R., Hogan, A., Grube, P., Lazzara, M., Bandy, A., Thornton, D., Berresheim, H., Bingemer, H., Hutterli, M., McConnell, J., Bales, R., Dibb, J., Buhr, M., Park, J., McMurry, P., Swanson, A., Meinardi, S., and Blake, D.: An overview of ISCAT 2000, Atmos. Environ., 38, 5363–5373, https://doi.org/10.1016/j.atmosenv.2004.05.037, 2004.

Ding, M., Tian, B., Ashley, M. C. B., Putero, D., Zhu, Z., Wang, L., Yang, S., Li, C., and Xiao, C.: Year-round record of near-surface ozone and O_3 enhancement events (OEEs) at Dome A, East Antarctica, Earth Syst. Sci. Data, 12, 3529–3544, https://doi.org/10.5194/essd-12-3529-2020, 2020.

Eisele, F., Davis, D., Helmig, D., Oltmans, S., Neff, W., Huey, G., Tanner, D., Chen, G., Crawford, J., and Arimoto, R.: Antarctic Tropospheric Chemistry Investigation (ANTCI) 2003 overview, Atmos. Environ., 42, 2749–2761, https://doi.org/10.1016/j.atmosenv.2007.04.013, 2008.

Falk, S. and Sinnhuber, B.-M.: Polar boundary layer bromine explosion and ozone depletion events in the chemistry–climate model EMAC v2.52: implementation and evaluation of AirSnow algorithm, Geosci. Model Dev., 11, 1115–1131, https://doi.org/10.5194/gmd-11-1115-2018, 2018.

685 Fernandez, R. P., Carmona-Balea, A., Cuevas, C. A., Barrera, J. A., Kinnison, D. E., Lamarque, J.-F., Blaszczak-Boxe, C., Kim, K., Choi, W., Hay, T., Blechschmidt, A.-M., Schönhardt, A., Burrows, J. P., and Saiz-Lopez, A.: Modeling the Sources and Chemistry of Polar Tropospheric Halogens (Cl, Br, and I) Using the CAM-Chem Global Chemistry-Climate Model, J. Adv. Model. Earth Syst., 11, 2259–2289, https://doi.org/10.1029/2019MS001655, 2019.

690 Frey, M. M., Stewart, R. W., McConnell, J. R., and Bales, R. C.: Atmospheric hydroperoxides in West Antarctica: Links to stratospheric ozone and atmospheric oxidation capacity, J. Geophys. Res., 110, D23301, https://doi.org/10.1029/2005JD006110, 2005.

Frey, M. M., Roscoe, H. K., Kukui, A., Savarino, J., France, J. L., King, M. D., Legrand, M., and Preunkert, S.: Atmospheric nitrogen oxides (NO and NO2) at Dome C, East Antarctica, during 695 the OPALE campaign, Atmos. Chem. Phys., 15, 7859–7875, https://doi.org/10.5194/acp-15-7859-2015, 2015.

Ghude, S. D., Jain, S. L., Arya, B. C., Kulkarni, P. S., Kumar, A., and Ahmed, N.: Temporal and spatial variability of surface ozone at Delhi and Antarctica, Int. J. Climatol., 26, 2227–2242, https://doi.org/10.1002/joc.1367, 2006.

700 Greenslade, J. W., Alexander, S. P., Schofield, R., Fisher, J. A., and Klekociuk, A. K.: Stratospheric ozone intrusion events and their impacts on tropospheric ozone in the Southern Hemisphere, Atmos. Chem. Phys., 17, 10269–10290, https://doi.org/10.5194/acp-17-10269-2017, 2017.

Griffiths, P. T., Murray, L. T., Zeng, G., Shin, Y. M., Abraham, N. L., Archibald, A. T., Deushi, 705 M., Emmons, L. K., Galbally, I. E., Hassler, B., Horowitz, L. W., Keeble, J., Liu, J., Moeini, O., Naik, V., O'Connor, F. M., Oshima, N., Tarasick, D., Tilmes, S., Turnock, S. T., Wild, O., Young, P. J., and Zanis, P.: Tropospheric ozone in CMIP6 simulations, Atmos. Chem. Phys., 21, 4187–4218, https://doi.org/10.5194/acp-21-4187-2021, 2021.

Helmig, D., Ganzeveld, L., Butler, T., and Oltmans, S. J.: The role of ozone atmosphere-snow 710 gas exchange on polar, boundary-layer tropospheric ozone – a review and sensitivity analysis, Atmos. Chem. Phys., 7, 15–30, https://doi.org/10.5194/acp-7-15-2007, 2007.

Honrath, R. E., Lu, Y., Peterson, M. C., Dibb, J. E., Arsenault, M. A., Cullen, N. J., and Steffen,

K.: Vertical fluxes of NOx, HONO, and HNO3 above the snowpack at Summit, Greenland, Atmos. Environ., 36, 2629–2640, https://doi.org/10.1016/S1352-2310(02)00132-2, 2002.

715   Jefferson, A., Tanner, D. J., Eisele, F. L., Davis, D. D., Chen, G., Crawford, J., Huey, J. W., Torres, A. L., and Berresheim, H.: OH photochemistry and methane sulfonic acid formation in the coastal Antarctic boundary layer, J. Geophys. Res. Atmos., 103, 1647–1656, https://doi.org/10.1029/97JD02376, 1998.

Jöckel, P., Tost, H., Pozzer, A., Brühl, C., Buchholz, J., Ganzeveld, L., Hoor, P., Kerkweg, A.,
720   Lawrence, M. G., Sander, R., Steil, B., Stiller, G., Tanarhte, M., Taraborrelli, D., van Aardenne, J., and Lelieveld, J.: The atmospheric chemistry general circulation model ECHAM5/MESSy1: consistent simulation of ozone from the surface to the mesosphere, Atmos. Chem. Phys., 6, 5067–5104, https://doi.org/10.5194/acp-6-5067-2006, 2006.

Jöckel, P., Kerkweg, A., Pozzer, A., Sander, R., Tost, H., Riede, H., Baumgaertner, A., Gromov,
725   S., and Kern, B.: Development cycle 2 of the Modular Earth Submodel System (MESSy2), Geosci. Model Dev., 3, 717–752, https://doi.org/10.5194/gmd-3-717-2010, 2010.

Jöckel, P., Tost, H., Pozzer, A., Kunze, M., Kirner, O., Brenninkmeijer, C. A. M., Brinkop, S., Cai, D. S., Dyroff, C., Eckstein, J., Frank, F., Garny, H., Gottschaldt, K.-D., Graf, P., Grewe, V., Kerkweg, A., Kern, B., Matthes, S., Mertens, M., Meul, S., Neumaier, M., Nützel, M.,
730   Oberländer-Hayn, S., Ruhnke, R., Runde, T., Sander, R., Scharffe, D., and Zahn, A.: Earth System Chemistry integrated Modelling (ESCiMo) with the Modular Earth Submodel System (MESSy) version 2.51, Geosci. Model Dev., 9, 1153–1200, https://doi.org/10.5194/gmd-9-1153-2016, 2016.

Jones, A. E.: An analysis of the oxidation potential of the South Pole boundary layer and the
735   influence of stratospheric ozone depletion, J. Geophys. Res., 108, 4565, https://doi.org/10.1029/2003JD003379, 2003.

Jones, A. E., Weller, R., Anderson, P. S., Jacobi, H.-W., Wolff, E. W., Schrems, O., and Miller, H.: Measurements of NOx emissions from the Antarctic snowpack, Geophys. Res. Lett., 28, 1499–1502, https://doi.org/10.1029/2000GL011956, 2001.

740   Jones, A. E., Wolff, E. W., Salmon, R. A., Bauguitte, S. J.-B., Roscoe, H. K., Anderson, P. S.,

Ames, D., Clemitshaw, K. C., Fleming, Z. L., Bloss, W. J., Heard, D. E., Lee, J. D., Read, K. A., Hamer, P., Shallcross, D. E., Jackson, A. V., Walker, S. L., Lewis, A. C., Mills, G. P., Plane, J. M. C., Saiz-Lopez, A., Sturges, W. T., and Worton, D. R.: Chemistry of the Antarctic Boundary Layer and the Interface with Snow: an overview of the CHABLIS campaign, Atmos. Chem. Phys., 8, 3789–3803, https://doi.org/10.5194/acp-8-3789-2008, 2008.

Jones, A. E., Anderson, P. S., Begoin, M., Brough, N., Hutterli, M. A., Marshall, G. J., Richter, A., Roscoe, H. K., and Wolff, E. W.: BrO, blizzards, and drivers of polar tropospheric ozone depletion events, Atmos. Chem. Phys., 9, 4639–4652, https://doi.org/10.5194/acp-9-4639-2009, 2009.

Jones, A. E., Wolff, E. W., Brough, N., Bauguitte, S. J.-B., Weller, R., Yela, M., Navarro-Comas, M., Ochoa, H. A., and Theys, N.: The spatial scale of ozone depletion events derived from an autonomous surface ozone network in coastal Antarctica, Atmos. Chem. Phys., 13, 1457–1467, https://doi.org/10.5194/acp-13-1457-2013, 2013.

Kerkweg, A., Jöckel, P., Pozzer, A., Tost, H., Sander, R., Schulz, M., Stier, P., Vignati, E., Wilson, J., and Lelieveld, J.: Consistent simulation of bromine chemistry from the marine boundary layer to the stratosphere – Part 1: Model description, sea salt aerosols and pH, Atmos. Chem. Phys., 8, 5899–5917, https://doi.org/10.5194/acp-8-5899-2008, 2008.

Kukui, A., Legrand, M., Ancellet, G., Gros, V., Bekki, S., Sarda-Estève, R., Loisil, R., and Preunkert, S.: Measurements of OH and RO2 radicals at the coastal Antarctic site of Dumont d'Urville (East Antarctica) in summer 2010–2011, J. Geophys. Res. Atmos., 117, https://doi.org/10.1029/2012JD017614, 2012.

Kumar, P., Kuttippurath, J., von der Gathen, P., Petropavlovskikh, I., Johnson, B., McClure-Begley, A., Cristofanelli, P., Bonasoni, P., Barlasina, M. E., and Sánchez, R.: The Increasing Surface Ozone and Tropospheric Ozone in Antarctica and Their Possible Drivers, Environ. Sci. Technol., 55, 8542–8553, https://doi.org/10.1021/acs.est.0c08491, 2021.

Legrand, M., Preunkert, S., Jourdain, B., Gallée, H., Goutail, F., Weller, R., and Savarino, J.: Year-round record of surface ozone at coastal (Dumont d'Urville) and inland (Concordia) sites in East Antarctica, J. Geophys. Res. Atmos., 114, https://doi.org/10.1029/2008JD011667, 2009.

Legrand, M., Preunkert, S., Savarino, J., Frey, M. M., Kukui, A., Helmig, D., Jourdain, B., Jones,

770   A. E., Weller, R., Brough, N., and Gallée, H.: Inter-annual variability of surface ozone at coastal
        (Dumont d'Urville, 2004–2014) and inland (Concordia, 2007–2014) sites in East Antarctica,
        Atmos. Chem. Phys., 16, 8053–8069, https://doi.org/10.5194/acp-16-8053-2016, 2016.

        Lelieveld, J. and Dentener, F. J.: What controls tropospheric ozone?, J. Geophys. Res. Atmos.,
        105, 3531–3551, https://doi.org/10.1029/1999JD901011, 2000.

775   Lelieveld, J., van Aardenne, J., Fischer, H., de Reus, M., Williams, J., and Winkler, P.:
        Increasing Ozone over the Atlantic Ocean, Science (80-.)., 304, 1483–1487,
        https://doi.org/10.1126/science.1096777, 2004.

        Mahajan, A. S., Li, Q., Inamdar, S., Ram, K., Badia, A., and Saiz-Lopez, A.: Modelling the
        impacts of iodine chemistry on the northern Indian Ocean marine boundary layer, Atmos. Chem.

780   Phys., 21, 8437–8454, https://doi.org/10.5194/acp-21-8437-2021, 2021.

        Masclin, S., Frey, M. M., Rogge, W. F., and Bales, R. C.: Atmospheric nitric oxide and ozone at
        the WAIS Divide deep coring site: a discussion of local sources and transport in West Antarctica,
        Atmos. Chem. Phys., 13, 8857–8877, https://doi.org/10.5194/acp-13-8857-2013, 2013.

        Mastrantonio, G., Malvestuto, V., Argentini, S., Georgiadis, T., and Viola, A.: Evidence of a

785   Convective Boundary Layer Developingon the Antarctic Plateau during the Summer, Meteorol.
        Atmos. Phys., 71, 127–132, https://doi.org/10.1007/s007030050050, 1999.

        Mihalikova, M. and Kirkwood, S.: Tropopause fold occurrence rates over the Antarctic station
        Troll (72° S, 2.5° E), Ann. Geophys., 31, 591–598, https://doi.org/10.5194/angeo-31-591-2013,
        2013.

790   Morgenstern, O., Zeng, G., Luke Abraham, N., Telford, P. J., Braesicke, P., Pyle, J. A.,
        Hardiman, S. C., O'Connor, F. M., and Johnson, C. E.: Impacts of climate change, ozone
        recovery, and increasing methane on surface ozone and the tropospheric oxidizing capacity, J.
        Geophys. Res. Atmos., 118, 1028–1041, https://doi.org/10.1029/2012JD018382, 2013.

        Murayama, S., Nakazawa, T., Tanaka, M., Aoki, S., and Kawaguchi, S.: Variations of

795   tropospheric ozone concentration over Syowa Station, Antarctica, Tellus B Chem. Phys.

Meteorol., https://doi.org/10.3402/tellusb.v44i4.15454, 1992.

Murazaki, K. and Hess, P.: How does climate change contribute to surface ozone change over the United States?, J. Geophys. Res. Atmos., 111, https://doi.org/10.1029/2005JD005873, 2006.

Nguyen, D.-H., Lin, C., Vu, C.-T., Cheruiyot, N. K., Nguyen, M. K., Le, T. H., Lukkhasorn, W.,
800   Vo, T.-D.-H., and Bui, X.-T.: Tropospheric ozone and NOx: A review of worldwide variation and meteorological influences, Environ. Technol. Innov., 28, 102809, https://doi.org/10.1016/j.eti.2022.102809, 2022.

Ojha, N., Pozzer, A., Akritidis, D., and Lelieveld, J.: Secondary ozone peaks in the troposphere over the Himalayas, Atmos. Chem. Phys., 17, 6743–6757, https://doi.org/10.5194/acp-17-6743-
805   2017, 2017.

Oltmans, S. J.: Surface ozone measurements in clean air, J. Geophys. Res. Ocean., 86, 1174–1180, https://doi.org/10.1029/JC086iC02p01174, 1981.

Oltmans, S. J. and Komhyr, W. D.: Surface ozone in Antarctica, J. Geophys. Res., 81, 5359–5364, https://doi.org/10.1029/JC081i030p05359, 1976.

810   Oltmans, S. J., Johnson, B. J., and Helmig, D.: Episodes of high surface-ozone amounts at South Pole during summer and their impact on the long-term surface-ozone variation, Atmos. Environ., 42, 2804–2816, https://doi.org/10.1016/j.atmosenv.2007.01.020, 2008.

Pozzer, A., de Meij, A., Pringle, K. J., Tost, H., Doering, U. M., van Aardenne, J., and Lelieveld, J.: Distributions and regional budgets of aerosols and their precursors simulated with the EMAC
815   chemistry-climate model, Atmos. Chem. Phys., 12, 961–987, https://doi.org/10.5194/acp-12-961-2012, 2012.

Pozzer, A., Reifenberg, S. F., Kumar, V., Franco, B., Kohl, M., Taraborrelli, D., Gromov, S., Ehrhart, S., Jöckel, P., Sander, R., Fall, V., Rosanka, S., Karydis, V., Akritidis, D., Emmerichs, T., Crippa, M., Guizzardi, D., Kaiser, J. W., Clarisse, L., Kiendler-Scharr, A., Tost, H., and
820   Tsimpidi, A.: Simulation of organics in the atmosphere: evaluation of EMACv2.54 with the Mainz Organic Mechanism (MOM) coupled to the ORACLE (v1.0) submodel, Geosci. Model Dev., 15, 2673–2710, https://doi.org/10.5194/gmd-15-2673-2022, 2022.

Preunkert, S., Ancellet, G., Legrand, M., Kukui, A., Kerbrat, M., Sarda-Estève, R., Gros, V., and Jourdain, B.: Oxidant Production over Antarctic Land and its Export (OPALE) project: An overview of the 2010–2011 summer campaign, J. Geophys. Res. Atmos., 117, https://doi.org/10.1029/2011JD017145, 2012.

Pringle, K. J., Tost, H., Message, S., Steil, B., Giannadaki, D., Nenes, A., Fountoukis, C., Stier, P., Vignati, E., and Lelieveld, J.: Description and evaluation of GMXe: a new aerosol submodel for global simulations (v1), Geosci. Model Dev., 3, 391–412, https://doi.org/10.5194/gmd-3-391-2010, 2010.

Reddy, N. S. K., N.V.P., K., K., R. G., G., B., and K., R. R.: Characteristics of atmospheric surface layer during winter season over Anantapur (14.62° N, 77.65° E), a semi-arid location in peninsular India, J. Atmos. Solar-Terrestrial Phys., 216, 105554, https://doi.org/10.1016/j.jastp.2021.105554, 2021.

Reifenberg, S. F., Martin, A., Kohl, M., Bacer, S., Hamryszczak, Z., Tadic, I., Röder, L., Crowley, D. J., Fischer, H., Kaiser, K., Schneider, J., Dörich, R., Crowley, J. N., Tomsche, L., Marsing, A., Voigt, C., Zahn, A., Pöhlker, C., Holanda, B. A., Krüger, O., Pöschl, U., Pöhlker, M., Jöckel, P., Dorf, M., Schumann, U., Williams, J., Bohn, B., Curtius, J., Harder, H., Schlager, H., Lelieveld, J., and Pozzer, A.: Numerical simulation of the impact of COVID-19 lockdown on tropospheric composition and aerosol radiative forcing in Europe, Atmos. Chem. Phys., 22, 10901–10917, https://doi.org/10.5194/acp-22-10901-2022, 2022.

Roeckner, E., Brokopf, R., Esch, M., Giorgetta, M., Hagemann, S., Kornblueh, L., Manzini, E., Schlese, U., and Schulzweida, U.: Sensitivity of Simulated Climate to Horizontal and Vertical Resolution in the ECHAM5 Atmosphere Model, J. Clim., 19, 3771–3791, https://doi.org/10.1175/JCLI3824.1, 2006.

Rolph, G., Stein, A., and Stunder, B.: Real-time Environmental Applications and Display sYstem: READY, Environ. Model. Softw., 95, 210–228, https://doi.org/10.1016/j.envsoft.2017.06.025, 2017.

Rosanka, S., Tost, H., Sander, R., Jöckel, P., Kerkweg, A., and Taraborrelli, D.: How non-equilibrium aerosol chemistry impacts particle acidity: the GMXe AERosol CHEMistry

(GMXe–AERCHEM, v1.0) sub-submodel of MESSy, Egusph. [preprint], https://doi.org/10.5194/egusphere-2023-2587, 2023.

Saiz-Lopez, A., Mahajan, A. S., Salmon, R. A., Bauguitte, S. J.-B., Jones, A. E., Roscoe, H. K., and Plane, J. M. C.: Boundary Layer Halogens in Coastal Antarctica, Science (80-.)., 317, 348–351, https://doi.org/10.1126/science.1141408, 2007.

Sanak, J., Lambert, G., and Ardouin, B.: Measurement of stratosphere-to-troposphere exchange in Antarctica by using short-lived cosmonuclides, Tellus B Chem. Phys. Meteorol., https://doi.org/10.3402/tellusb.v37i2.15005, 1985.

Schönhardt, A., Begoin, M., Richter, A., Wittrock, F., Kaleschke, L., Gómez Martín, J. C., and Burrows, J. P.: Simultaneous satellite observations of IO and BrO over Antarctica, Atmos. Chem. Phys., 12, 6565–6580, https://doi.org/10.5194/acp-12-6565-2012, 2012.

Seinfeld, J. H. and Pandis, S. N.: Atmospheric Chemistry and Physics: From Air Pollution to Climate Change, 88–90 pp., https://doi.org/10.1063/1.882420, 1998.

Simpson, W. R., von Glasow, R., Riedel, K., Anderson, P., Ariya, P., Bottenheim, J., Burrows, J., Carpenter, L. J., Frieß, U., Goodsite, M. E., Heard, D., Hutterli, M., Jacobi, H.-W., Kaleschke, L., Neff, B., Plane, J., Platt, U., Richter, A., Roscoe, H., Sander, R., Shepson, P., Sodeau, J., Steffen, A., Wagner, T., and Wolff, E.: Halogens and their role in polar boundary-layer ozone depletion, Atmos. Chem. Phys., 7, 4375–4418, https://doi.org/10.5194/acp-7-4375-2007, 2007.

Soni, V. K., Sateesh, M., Das, A. K., and Peshin, S. K.: Progress in meteorological studies around Indian stations in Antarctica, Proc. Indian Natl. Sci. Acad., 83, https://doi.org/10.16943/ptinsa/2017/48954, 2017.

Stein, A. F., Draxler, R. R., Rolph, G. D., Stunder, B. J. B., Cohen, M. D., and Ngan, F.: NOAA's HYSPLIT Atmospheric Transport and Dispersion Modeling System, Bull. Am. Meteorol. Soc., 96, 2059–2077, https://doi.org/10.1175/BAMS-D-14-00110.1, 2015.

Stohl, A., Bonasoni, P., Cristofanelli, P., Collins, W., Feichter, J., Frank, A., Forster, C., Gerasopoulos, E., Gäggeler, H., James, P., Kentarchos, T., Kromp-Kolb, H., Krüger, B., Land, C., Meloen, J., Papayannis, A., Priller, A., Seibert, P., Sprenger, M., Roelofs, G. J., Scheel, H. E.,

Schnabel, C., Siegmund, P., Tobler, L., Trickl, T., Wernli, H., Wirth, V., Zanis, P., and Zerefos, C.: Stratosphere-troposphere exchange: A review, and what we have learned from STACCATO, J. Geophys. Res. Atmos., 108, https://doi.org/10.1029/2002JD002490, 2003.

Taraborrelli, D., Cabrera-Perez, D., Bacer, S., Gromov, S., Lelieveld, J., Sander, R., and Pozzer, A.: Influence of aromatics on tropospheric gas-phase composition, Atmos. Chem. Phys., 21, 2615–2636, https://doi.org/10.5194/acp-21-2615-2021, 2021.

Tarasick, D. W. and Bottenheim, J. W.: Surface ozone depletion episodes in the Arctic and Antarctic from historical ozonesonde records, Atmos. Chem. Phys., 2, 197–205, https://doi.org/10.5194/acp-2-197-2002, 2002.

Tian, B., Ding, M., Putero, D., Li, C., Zhang, D., Tang, J., Zheng, X., Bian, L., and Xiao, C.: Multi-year variation of near-surface ozone at Zhongshan Station, Antarctica, Environ. Res. Lett., 17, 044003, https://doi.org/10.1088/1748-9326/ac583c, 2022.

Toyota, K., McConnell, J. C., Lupu, A., Neary, L., McLinden, C. A., Richter, A., Kwok, R., Semeniuk, K., Kaminski, J. W., Gong, S.-L., Jarosz, J., Chipperfield, M. P., and Sioris, C. E.: Analysis of reactive bromine production and ozone depletion in the Arctic boundary layer using 3-D simulations with GEM-AQ: inference from synoptic-scale patterns, Atmos. Chem. Phys., 11, 3949–3979, https://doi.org/10.5194/acp-11-3949-2011, 2011.

Wang, H., Lu, X., Jacob, D. J., Cooper, O. R., Chang, K.-L., Li, K., Gao, M., Liu, Y., Sheng, B., Wu, K., Wu, T., Zhang, J., Sauvage, B., Nédélec, P., Blot, R., and Fan, S.: Global tropospheric ozone trends, attributions, and radiative impacts in 1995–2017: an integrated analysis using aircraft (IAGOS) observations, ozonesonde, and multi-decadal chemical model simulations, Atmos. Chem. Phys., 22, 13753–13782, https://doi.org/10.5194/acp-22-13753-2022, 2022.

Winkler, P., Brylka, S., and Wagenbach, D.: Regular fluctuations of surface ozone at Georg-von-Neumayer station, Antarctica, Tellus B, 44, 33–40, https://doi.org/10.1034/j.1600-0889.1992.00003.x, 1992.

Yang, X., Cox, R. A., Warwick, N. J., Pyle, J. A., Carver, G. D., O'Connor, F. M., and Savage, N. H.: Tropospheric bromine chemistry and its impacts on ozone: A model study, J. Geophys. Res. Atmos., 110, https://doi.org/10.1029/2005JD006244, 2005.

Young, P. J., Naik, V., Fiore, A. M., Gaudel, A., Guo, J., Lin, M. Y., Neu, J. L., Parrish, D. D., Rieder, H. E., Schnell, J. L., Tilmes, S., Wild, O., Zhang, L., Ziemke, J., Brandt, J., Delcloo, A., Doherty, R. M., Geels, C., Hegglin, M. I., Hu, L., Im, U., Kumar, R., Luhar, A., Murray, L., Plummer, D., Rodriguez, J., Saiz-Lopez, A., Schultz, M. G., Woodhouse, M. T., and Zeng, G.:

910   Tropospheric Ozone Assessment Report: Assessment of global-scale model performance for global and regional ozone distributions, variability, and trends, Elem. Sci. Anthr., 6, 10, https://doi.org/10.1525/elementa.265, 2018.